Organic Solar Cells Fabrication and Optimization through Hole Transport Layer (HTL) Treatments

Katerina Anagnostou

1/9/2017
University of Crete, Department of Chemistry-NANOgroup University of Applied Sciences, Crete

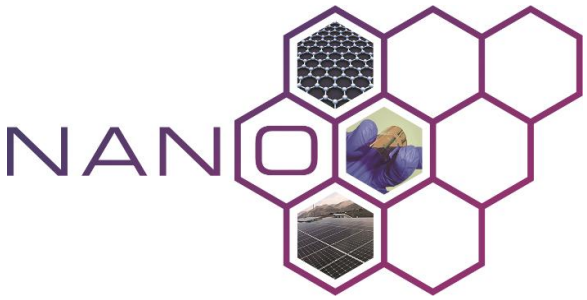

Diploma Thesis

Preface:

The presented Diploma thesis was carried out in the laboratory of The Nanomaterials & Advanced Electronics (NANO) Group at the University of Applied Sciences (UAS) in Herakleion, Crete from February 2017 to October 2017 under supervision and guidance of Prof. Athanasios Koutsolelos (Department of Chemistry at the University of Crete), Prof. Emmanuel Kymakis and Dr. Minas Stylianakis (UAS of Crete).

Abstract

The purpose of this diploma thesis is the fabrication Organic Solar Cells (OSCs) with optimized performance. More specifically, the conventional poly(3,4-ethylenedioxythiophene):poly(styrene sulfonate) (PEDOT:PSS), which mainly acts in OSCs as the hole transport Layer (HTL) and electron blocking layer (EBL), will be treated in several ways, in order to tune its properties (optoelectronic, energy levels etc.) and therefore improve the device performance. The project consists of a two-step PEDOT:PSS treatment: a) the direct incorporation of tetrafluoroethylene-perfluoro-3,6-dioxa-4-methyl-7-octene-sulfonic acid copolymer (PFI) and b) the immersion in dimethyl sulfoxide (DMSO). In this context, the optimum fabrication process was investigated, while OSC device characteristics (Short-Circuit Current Density (J_{SC}), Open-Circuit Voltage (V_{OC}), Fill Factor (FF) and power convention efficiency (PCE) were determined using a solar simulator. Hole mobility (μ_h) of each HTL was also calculated. The morphology and surface roughness (R_{MS}) of each HTL was investigated using Atomic Force Spectroscopy (AFM). Results showed that the values of PCE, J_{SC}, FF and μ_h were increased via treatment of PEDOT:PSS with PFI. This increase was further enhanced with the additional treatment with DMSO. The V_{OC} value remained constant for all three fabricated devices, while the value of surface roughness (R_{MS}) showed an increase for the PFI treated HTL and an even further increase for the PFI-DMSO treated HTL.

Περίληψη:

Σκοπός της παρούσας διπλωματικής εργασίας είναι η κατασκευή Οργανικών Φωτοβολταϊκών Κελιών (Organic Solar Cells, OSCs) με βελτιωμένη επίδοση. Ειδικότερα, το υλικό (3,4-ethylenedioxythiophene):poly(styrene sulfonate) (PEDOT:PSS) που χρησιμοποιείται συμβατικά στα OSCs ως transport Layer (HTL)

και παράλληλα ως electron blocking layer (EBL) υπόκεινται σε κατεργασία με αποτέλεσμα τον συντονισμό των ιδιοτήτων του (οπτικο-ηλεκτρικές ιδιότητες, ενεργειακά επίπεδα κλπ) και κατ' επέκταση την βελτίωση της επίδοσης της φωτοβολταϊκής συσκευής. Η κατεργασία του PEDOT:PSS πραγματοποιείται με μία μέθοδο δυο βημάτων: α) Η άμεση ενσωμάτωση του συμπολυμερούς tetrafluoroethylene-perfluoro-3,6-dioxa-4-methyl-7-octene-sulfonic acid (PFI) και β) καταβύθιση σε λουτρό dimethyl sulfoxide (DMSO). Η βέλτιστη μέθοδος κατασκευής φωτοβολταϊκής συσκευής διερευνήθηκε μετρώντας και συγκρίνοντας τα χαρακτηριστικά: Πυκνότητα ρεύματος κλειστού κυκλώματος (J_{SC}), τάση ρεύματος ανοιχτού κυκλώματος (V_{OC}), παράγοντας πλήρωσης (FF), και απόδοση μετατροπής ρεύματος (PCE). Οι παραπάνω μετρήσεις λαμβάνονται με χρήση προσομοιωτή ηλιακής ακτινοβολίας. Στη συνέχεια μετρήθηκε η τιμή της κινητικότητας οπών (μ_h) για κάθε συσκευή, διερευνήθηκε η μορφολογία του κάθε HTL χρησιμοποιώντας Atomic Force Spectroscopy (AFM) και, τέλος, μετρήθηκε και η τραχύτητα επιφάνειας (R_{MS}). Τα αποτελέσματα έδειξαν αύξηση στη τιμή των PCE, J_{SC}, FF και μ_h για το HTL που υπέστη κατεργασία με PFI και ακόμη μεγαλύτερη αύξηση στις ίδιες τιμές για το HTL που υπέστη περαιτέρω κατεργασία με DMSO. Οι τιμή του V_{OC} παρέμεινε σταθερή και για τις τρεις μετρούμενες φωτοβολταϊκές συσκευές, ενώ η τιμή της τραχύτητας επιφάνειας έδειξε αύξηση για το HTL που είχε κατεργαστεί με PFI και περαιτέρω αύξηση για το HTL που είχε κατεργαστεί με PFI και DMSO.

Acknowledgements:

I would like to thank my parents and my grandparents, whose support and encouragement have been of the most important value to me throughout my academic progress. I would also like to thank Prof. Athanasios Koutsolelos, Prof. Emmanuel Kymakis and Dr. Minas Stylianakis for giving me the opportunity to carry out my diploma thesis at NANOgroup laboratories and to work on a whole new research field, thus broadening my horizons. A special thank you to Miron Krassas who proved to be an excellent mentor throughout this diploma thesis, offering guidance and support whenever needed.

Abbreviations:

OSCs	Organic Solar Cells
OPVs	Organic Photovoltaics
I_{SC}	Short Circuit Current
J_{SC}	Short Circuit Current Density
V_{OC}	Open Circuit Voltage
FF	Fill Factor
PCE	Power Conventional Efficiency
μ_h	Hole mobility
HTL/EBL	Hole transport layer/Electron blocking layer
ETL/HBL	Electron transport layer/Hole blocking layer
AL	Active layer
TCO	Transparent conducting oxide
PTB_7	Poly[[4,8-bis[(2-ethylhexyl)oxy]benzo[1,2-b:4,5-b']dithiophene-2,6-diyl][3-fluoro-2-[(2-ethylhexyl)carbonyl]thieno[3,4-b]thiophenediyl]]
$PC_{60}BM$	Phenyl-C60-butyric acid methyl ester
DIO	3,3'-dioctadecyloxacarbocyanine
DCB	Dichlorobenzene
CB	Chlorobenzene
ITO	Indium tin oxide
PEDOT:PSS	Poly(3,4-ethylenedioxythiophene) poly(styrene sulfonate)
PFI	Tetrafluoroethylene-perfluoro-3,6-dioxa-4-methyl-7-octenesulfonic acid copolymer
DMSO	Dimethyl Sulfoxide

Table of Contents:

Chapter 5: Experimental Procedure

Chapter 6: Results and discussion

Chapter 1: Introduction

1.1. Alternative Energy Resources:

There are a plethora of reasons alternative, renewable energy is essential to human life and the environment in today's world. The first and main reason governments and businesses are keen to move to renewable energies as soon as possible is that fossil fuels are a finite resource. We may or may not have reached peak oil - the point at which demand outstrips supply. Politicians and economists have debated over this for decades. Either way, fossil fuels will run out eventually and it will take some 10,000,000 years to replenish what we have used in around 150 years. As the human population increases, our *rate* of consumption of these fossil fuels also increases and it is becoming increasingly difficult to locate and extract new sources. Whether we have 1 year or 100 years left of oil, many argue that what is left should remain in the ground because it is not sustainable - it will run out eventually and so we should prepare for a post-fossil fuel world now.

The second reason is climate change due to global warming and the carbon emissions which exacerbate this phenomenon. Most renewable energy sources, and the technology used to harness them, are low carbon emission. In most cases, once installed they have minimal or no carbon output and can still provide our energy needs. We can never go fully carbon neutral as it takes resources to i.e. make a solar panel, build a dam and so on, but these alternative energy resources are crucial to the reduction of our carbon footprint.

Other reasons for implementing alternative energy are worth mentioning, such as economic stability: Since alternative energy sources are inexhaustible (i.e. solar and wind power), these sources may help stabilize energy prices in the future. Furthermore, if humanity turns towards non-fossil fuel energy sources, environmental damage and public health risks caused by fracking and drilling will be avoided.

The most common forms of renewable energy are wind power, hydroelectricity, geothermal energy, bio-fuel, biomass and of source, the energy source of interest in this diploma thesis, solar power[1].

1.2. Solar Energy:

Solar power is arguably one of the best-known renewable energy sources. The most obvious advantage of solar energy is that it is practically infinite since it will last as long as the sun lasts-this time has been estimated to be 5 billion years. Unlike fossil fuel and oil, solar energy cannot run out. It can be harnessed in every area of the world and is available every day.

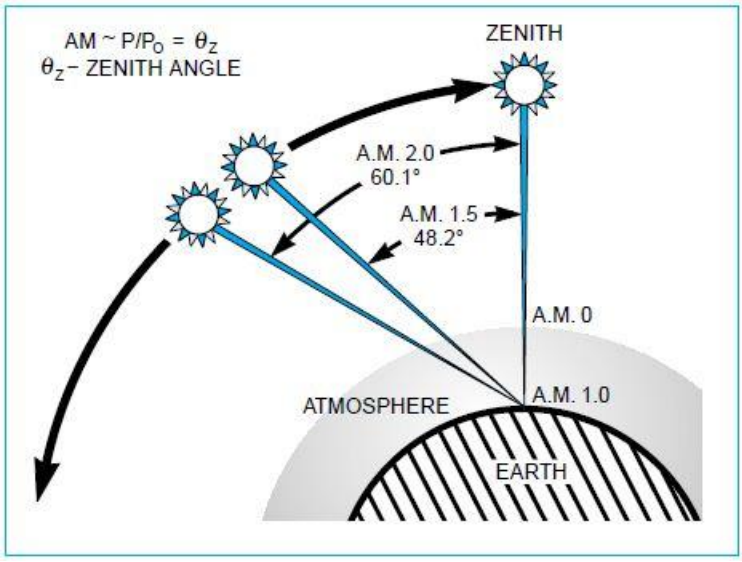

Figure 1.1 Solar radiation entering the Earth's atmosphere

Every second the Sun releases huge amounts of energy into space. Part of that energy enters Earth's atmosphere in the form of radiation and is essential for all life on our planet. Because our atmosphere does not maintain the same consistency everywhere, the radiation reaching the Earth's surface differs from place to place. Furthermore, because of Earth's shape, sunbeams reach the surface at different angles, while the distance between the Sun and the Earth is not stable. Due to these facts, a *solar constant* has been determined: The solar constant is the solar electromagnetic radiation per unit area ($1m^2$) that would be incident on a plane perpendicular to the rays, at a distance of one astronomical unit (AU) from the Sun (roughly the mean distance from the Sun to the Earth). The solar constant is measured as being G_{SC}= 1361 W/m^2.

The most important parameter which determines sun radiation under clear sky conditions is the distance which the sunlight has to travel through the atmosphere. This distance is at a minimum when the sun is at the point of zenith-directly above the Earth. The real length that sunlight travels at this

minimum distance is referred to as air mass 1 (AM 1). When the sun is positioned at an angle (θ) towards the zenith position, the air mass is given by the equation:

$$AM=(\cos\theta)^{-1} \quad (1.1)$$

According to this equation, if the sun is positioned at a 60° angle, then the suns radiation is referred to as AM2. Sunlight in space or in zero atmosphere is referred to as AM0.

For comparable measurements during the characterisation of photovoltaic devices, a standard sunlight spectrum must be set. Solar radiation AM 1.5 (at an angle of 48.2°) constitutes a typical sunlight spectrum on the Earth's surface on a sunlit day and is used during the characterisation of solar collecting devices.
Although the term AM1 or AM1.5 is often used to refer to standard spectra, the relative optical air mass (AM) is a geometrical quantity and can be obtained by taking the secant of the zenith angle. For AM1, the zenith angle is 0°. The relative optical air mass can be pressure-corrected to an absolute air mass by multiplying by the barometric pressure and dividing by the sea level pressure. The global and direct terrestrial reference spectra are often referred to as AM1.5 G and AM1.5 D, respectively. Many groups often just refer to the reference spectrum as AM1.5. This can be confusing without a reference because numerous different AM1.5 reference spectra have been proposed and used in the past. It should be noted that neither the direct reference spectrum nor the global reference spectrum actually integrates to exactly 1000 W/m^2 [2]. The global reference spectrum integrates to approximately 963 W/m^2 and the direct reference spectrum integrates to approximately 768 W/m^2 (Figure 1.2).

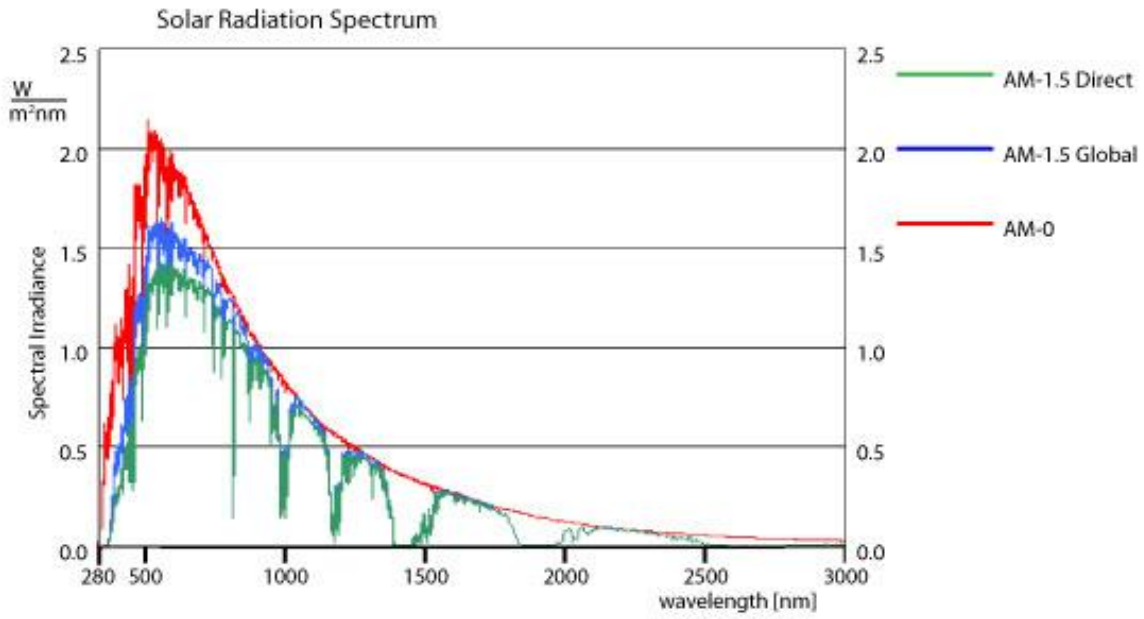

Figure 1.2 Global, Direct, and AM0 reference spectra.

The PV community has arbitrarily taken the term "one sun" to mean a total irradiance of 1000 W/m^2 (100mW/cm^2). In fact, the spectral irradiance of the global reference spectrum normalized to 1000 W/m^2 in Figure 1.2 exceeds the AM0 spectral irradiance in the infrared, which is not physically possible without concentration.

During the characterization of the OPV devices in this project, a solar simulator is used and it is set to illuminate devices under AM 1.5 conditions, as seen in Chapter 5.

1.3. The photovoltaic effect:

Photovoltaic devices have the ability to convert part of the electromagnetic radiation they absorb through sunlight into electric energy.

Sunlight consists of particles known as photons - small bundles of electromagnetic radiation or energy. The amount of energy which photons carry depends on the emission frequency of the light. Of the electromagnetic energy emitted from the sun, approximately 50% lies in the ultraviolet (UV) region, about 40% in the visible region and about 10% in the infra red (IR) region.

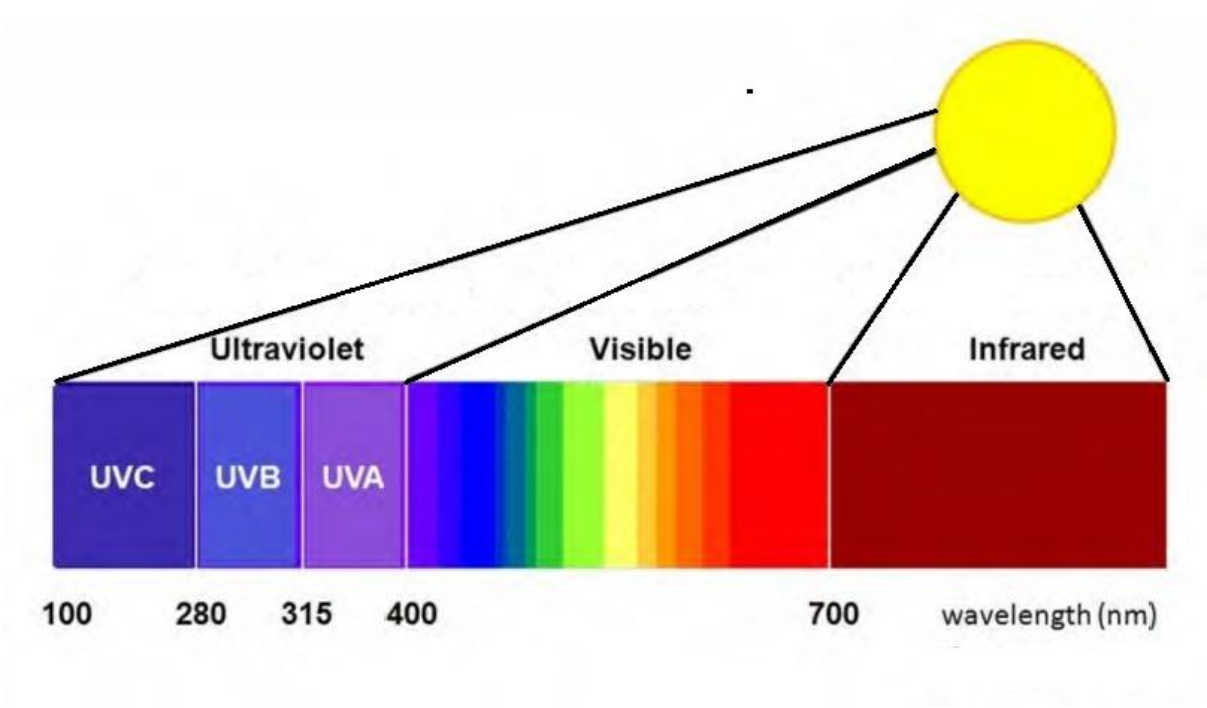

Figure 1.3 Radiation spectra of sunlight.

Photons in the visible and IR region carry enough energy to excite electrons in semiconductor materials which may lead to sufficient production of electric charges.
The photovoltaic effect which occurs in solar cells works as follows: Solar cells are composed of two different types of semiconductor - a p-type and an n-type - that are joined together to create a p-n junction. By joining these two types of semiconductors, an electric field is formed in the region of the junction as electrons move to the positive p-side and electron holes move to the negative n-side. This field causes negatively charged particles to move in one direction and positively charged particles in the other direction. [3] The excited electrons and the holes they leave behind are collected at separate electrodes creating electric potential.
There are four basic steps in the photovoltaic process[4]:

a) Light absorption
b) Generation of electric charges
c) Transfer of these electric charges
d) Collection of electric charges

The key component in the occurrence of the photovoltaic effect is the presence of a material with semi-conductive properties. The energy generated from this effect depends, among other things, on the pathways

through which electric charges are carried as well as the energy band gap of the semi-conducting materials that are used.

1.4. Generations of Solar Cells

From the discovery of the photovoltaic effect by Edmond Becquerel in 1839 to the development of the first marketable solar panel, photovoltaic technology has come a long way and is still making strides in the development of new, state of the art solar cell technologies and the optimisation of efficiency, cost and stability.

Solar panels are a lot cheaper and more efficient than they were in the 1980's when they first entered the market. However, the improvement of these devices is being widely investigated with the goal of lowering the manufacturing costs and increasing the efficiency. The still unreachable goal of all research groups worldwide is to construct a solar cell which would be power efficient and stable, with low cost manufacturing and a long life span. Those three parameters (efficiency, cost, lifetime) are what characterize and classify every solar device and all three of them are equally important for an efficient solar device.

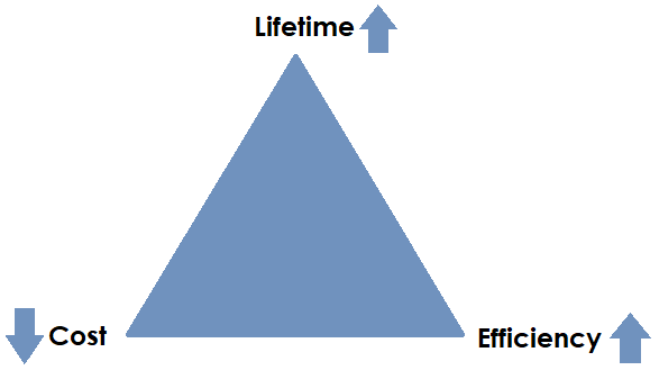

Figure 1.4 the three parameters that set the goals of solar cell development: Low cost, high efficiency and a long life span.

The solar cells which have been developed thus far can be categorised into three generations, as listed below[5]

1.4.1. First Generation:

Generally first generation solar cells are based on Silicon (Si). Though this technology has high conversion efficiency (typically demonstrate a performance about 15-20%[6]), the availability of Silicon is intricate because of its high cost. Furthermore, the fabrication process of the silicon based solar cell is complex. Si solar cells are currently the most efficient solar cells available for residential use and account for around 86 percent of all the solar panels sold around the world[7]. The benefits of this solar cell technology lie in their good performance, as well as their high stability. However, they are rigid, they require a lot of energy in production and are more at risk to lose some of their efficiency at higher temperatures (hot sunny days), than thin-film solar cells.

Silicon based cells used in the production of solar panels for residential use, are divided into four groups depending on the form of the silicon used.

a) Monocrystalline Silicon Cells

The oldest solar cell technology and still the most popular and efficient are solar cells made from thin wafers of silicon. These are called monocrystalline solar cells because the cells are sliced from large single crystals that have been painstakingly grown under carefully controlled conditions. Typically, the cells are a few inches across, and a number of cells are laid out in a grid to create a panel.

Figure 1.5 The monocrystalline silicon solar cells that make up a solar panel.

Relative to the other types of cells, they have a higher efficiency (up to 24.7%)[8], meaning that more electricity can be obtained from a given area of panel. However, growing large crystals of pure silicon is a difficult and very energy-intensive process, so the production costs for this type of panel are historically the highest of all the solar panel types. Production methods have improved though, and prices for raw silicon as well as to build panels from monocrystalline solar cells have fallen a great deal over the years,

partly driven by competition as other types of panel have been produced.

b) Polycrstalline Silicon Cells

It is cheaper to produce silicon wafers in moulds from multiple silicon crystals rather than from a single crystal as the conditions for growth do not need to be as tightly controlled. In this form, a number of interlocking silicon crystals grows together. Panels based on these cells are cheaper per unit area than monocrystalline panels - but they are also slightly less efficient (up to 20.3%)[9].

c) Amorphous Silicon Cells

Instead of growing silicon crystals as is done in making the two previous types of solar cells, silicon is deposited in a very thin layer on to a backing substrate – such as metal, glass or even plastic. Sometimes several layers of silicon, doped in slightly different ways to respond to different wavelengths of light, are laid on top of one another to improve the efficiency. The production methods are complex, but less energy intensive than crystalline panels, and prices have been coming down as panels are mass-produced using this process.

One advantage of using very thin layers of silicon is that the panels can be made flexible. The disadvantage of amorphous panels is that they are much less efficient per unit area (up to 10.1%) and are generally not suitable for roof installations you would typically need nearly double the panel area for the same power output. However, for a given power rating, they do perform better at low light levels than crystalline panels, making them suitable for the winter months and avoiding the decline of efficiency with the rise of temperature. Another key characteristic of thin film solar cells is their high flexibility, which makes them suitable in building integrated PVs (e.g., roofing shingles) or for use on curved surfaces.

d) Hybrid Silicon Cells

One recent trend in the industry is the emergence of hybrid silicon cells and several companies are now exploring ways of combining different materials to make solar cells with better efficiency, longer life, and at reduced costs.

1.4.2. Second Generation Solar Cells:

Second-generation solar cells are also called *thin-film* solar cells because they are made from layers of semiconductor materials only a few micrometers thick. The combination of using less material and lower cost manufacturing processes allow the manufacturers of solar panels made from this type of technology to produce and sell panels at a much lower cost. However, even though they have lower production cost than first generation solar cells but, they also have lower efficiencies. The superior characteristic of thin-films offers the great property of flexibility which dictates the availability of almost any shape surface application. Thin-film technology has spurred lightweight, aesthetically pleasing solar innovations such as solar shingles and solar panels.

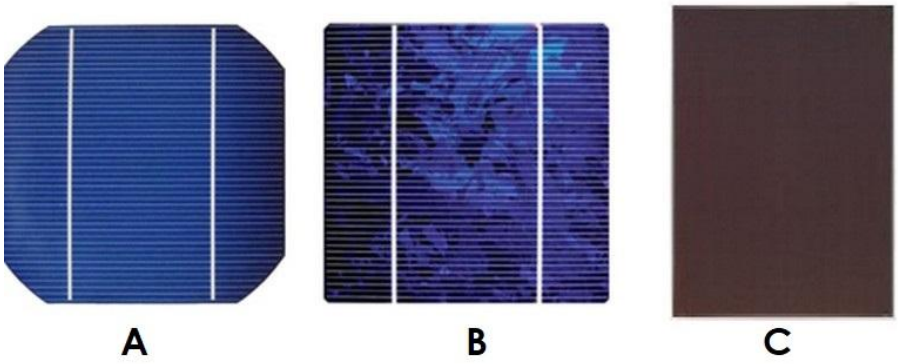

Figure 1.6 From left to right: Monocrystalline silicon, polycrystalline silicon and thin film solar cell.

Most successful materials for 2G are amorphous silicon, CuIn(Ga)Se2 (CIGS), CdTe/CdS, which are being deposited on thin substrates. Devices based on these materials can deliver lab efficiencies up to 20% (ZSW 21.7%, First Solar 21.5%), but the module efficiencies are reaching only 14 % due to difficulties in producing large scale uniform films[10]. Although thin film technology can significantly decrease the prices for PVs, 2G solar cells will also hit certain price limits per watt due to efficiency limits and the material costs.

1.4.3. Third Generation Solar Cells:

The third generation (or emerging PVs) is generation that goes beyond silicon-based solar cells. It includes solar cells which do not use the p-n junction structure that is used in traditional semiconductor, Si-based solar cells. This

new generation of solar cells are being made from a variety of new materials besides silicon, including nanotubes, silicon wires, solar inks using conventional printing press technologies, organic dyes, and conductive plastics. The goal of course is to improve on the solar cells already commercially available by making solar energy more efficient over a wider band of solar energy (e.g., including infrared), less expensive so it can be made available to a larger public and to develop more applications for this branch of technology.

Third generation contains a wide range of potential and efficient solar innovations including: Dye-sensitized nanocrystalline TiO_2 solar cells (DSSCs)[11],[12], molecular organic solar cells (MOSCs) and polymer organic solar cells (PSCs)[13].

a) Dye-sensitized solar cells (DSSCs): are based on combination of dyes with metal oxides and electrolyte. The efficiencies of DSSC are in the range of 12% (Figure…) for small lab scale devices, while the lifetime of the devices is rather low compared to inorganic solar cells. In a DSSC, an organic dye adsorbed at the surface of an inorganic wideband gap semiconductor is used for absorption of light and injection of the photo-excited electron into the conduction band of the semiconductor. The research on DSSCs gained considerable impulse, when Grätzel and co-workers greatly improved the interfacial area between the organic donor and inorganic acceptor by using nanoporous titanium dioxide (TiO_2)[14].

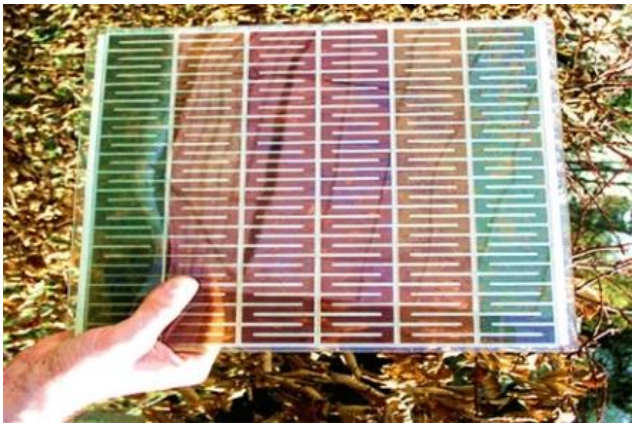

Figure 1.7 A Dye-sensitized solar cell.

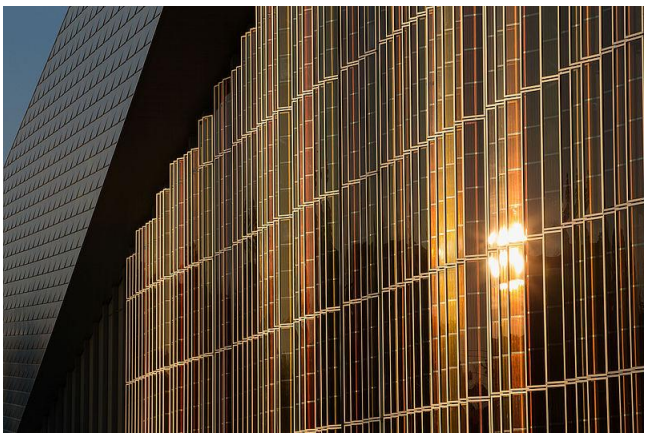

Figure 1.8 Grätzel cells on the SwissTech Convention Center.

b) Molecular organic solar cells: Small molecular semiconductors can be generally classified as hole or electron transporting (p-type or n-type) materials according to the type of orderly transferring charge carriers, under a given set of conditions, stemming from removal of electrons from the filled molecular orbitals or from the addition of electrons to empty orbitals, respectively. Many small molecular p-type semiconductors have been studied for decades. Among these molecules, only a small fraction has been applied successfully as electron donors in OPV devices due to the various optical, electrical, and stability requirements demanded of the chosen materials. The properties of materials, such as hole mobility (i.e., the distance over which holes are transported per second under the unit electric field), exciton diffusion length, thin film morphology, frontier energy level alignment, band gap, and absorption coefficient, all greatly affect the performance of OPV device. In this section, some representative small molecular donors such as dyes, fused acenes, oligothiophenes, and triphenylamine-based molecules used in the active layer of OPVs are described and discussed[15].

c) Polymer Organic Solar Cells: OSC technologies are under continuous development as that interest stems from their great characteristics including: fabrication with flexible substrates, lightweight, and production by inexpensive, low temperature deposition techniques such as spin-coating and printing, solution processed, transparent and use of cheap raw materials. Especially in the last decade the field of OPVs has been growing really fast and showing promising potential for rather cheap PV technology. For that reason, in recent years OPVs became one of the most fascinating fields of research. Historically,

anthracene was the first organic compound in which photoconductivity have been observed by Pochettino in 1906[16] and which started a new era for studying organic compounds for electronic applications. There are three subcategories of polymer organic solar cells:

- ***Single-layer*** Single layer organic photovoltaic cells are the simplest form. The first attempts to create all-organic solar cells were made by sandwiching a layer of organic electronic materials between two metallic conductors (Fig. 1.8), typically a layer of indium tin oxide (ITO) with high work function and a layer of low work function metal such as Aluminum (Al), Magnesium (Mg) or Calcium (Ca). In these cells, the photovoltaic properties strongly depend on the nature of the electrodes. Heavily doped conjugated materials resulted in reasonable power conversion efficiencies up to 0.3%.

- ***Bi-layer*** In the double-layer structure (Fig. 1.9) the photo-excitations in the photoactive material have to reach the p-n interface where charge transfer can occur, before the excitation energy of the molecule is lost via intrinsic radiative and non-radiative decay processes to the ground state. Because the exciton diffusion length of the organic material is in general limited to 5-10nm, only absorption of light within a very thin layer around the interface contributes to the photovoltaic effect. This limits the performance of double-layer devices, because such thin layer can impossibly absorb all the light. A strategy to improve the efficiency of the double-layer cell is related to structural organization of the organic material to extend the exciton diffusion length and, therefore, create a thicker photoactive interfacial area.

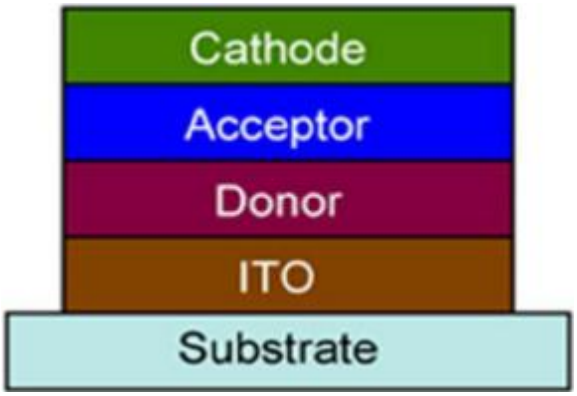

Figure 1.9 A typical bi-layer solar cell structure.

- ***Bulk Heterojunction*** The bulk heterojunction is presently the most widely used photoactive layer. The name bulk-heterojunction solar cell has been chosen, because the interface (heterojunction) between both components is all over the bulk (Figure 1.10), in contrast to the classical (bi-layer) heterojunction. As a result of the intimate mixing, the interface where charge transfer can occur has increased enormously. The exciton (hole-excited electron pair), created after the absorption of light, has to diffuse towards this charge-transfer interface for charge generation to occur. The diffusion length of the exciton in organic materials, however, is typically 5-10 nm[17]. This means that for efficient charge generation after absorption of light, each exciton (hole-electron pair) has to find a Donor:Acceptor (D:A) interface within a few nm to dissociate otherwise, it will be lost (emission/losses) without charge generation. An intimate bi-continuous network of donor and acceptor materials in the nanometer range should suppress exciton loss prior to charge generation. Control of morphology is not only required for a large charge-generating interface and suppression of exciton loss, but also to ensure percolation pathways for both electron and hole transport to the collecting electrodes respectively. In combining electron donating (p-type) and electron accepting (n-type) materials in the active layer of a solar cell, care must be taken that excitons created in either material can diffuse to the interface, to enable charge separation. Due to their short lifetime and low mobility, the limited diffusion length of excitons in organic semiconductors, imposes an important condition to efficient charge generation. Anywhere in the active layer, the distance to the interface should be on the order of the exciton diffusion length. Despite their high absorption coefficients, exceeding 105 cm^{-1}, a 20 nm double layer of donor and acceptor materials (bi-layer) would not be optical dense, allowing most photons to pass freely. The solution to this dilemma is elegantly simple. By simple mixing the p and n-type materials and relying on the intrinsic tendency of polymer materials to phase separate on a nanometer dimension, junctions throughout the bulk of the material are created that ensure quantitative dissociation of photo-generated excitons, irrespective of the thickness. Polymer-fullerene solar cells were among the first to utilize this bulk-heterojunction principle. Nevertheless, this attractive solution poses a new challenge. Photo-generated charges must be able to migrate to the collecting electrodes through this intimately mixed blend. Because holes are

transported by the p-type semiconductor and electrons by the n-type material, these materials should be preferably mixed into a bi-continuous, interpenetrating network in which inclusions, barrier layers are avoided. When such a bulk-heterojunction is deposited on an ITO substrate and capped with a metal back electrode, working photovoltaic cells can be obtained.

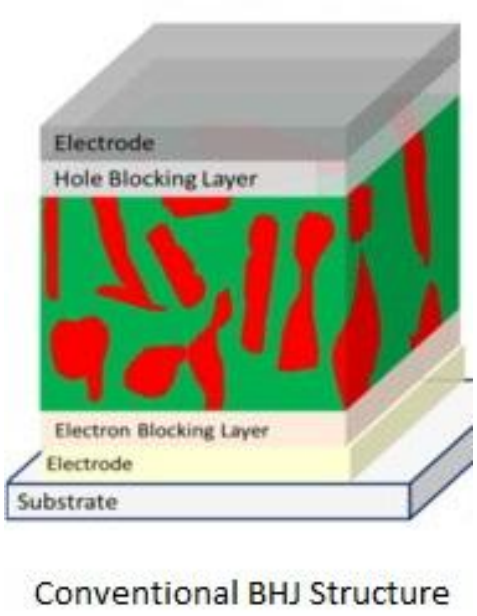

Figure 1.10 A typical conventional structure of a Bulk-heterojunction (BHJ) solar cell.

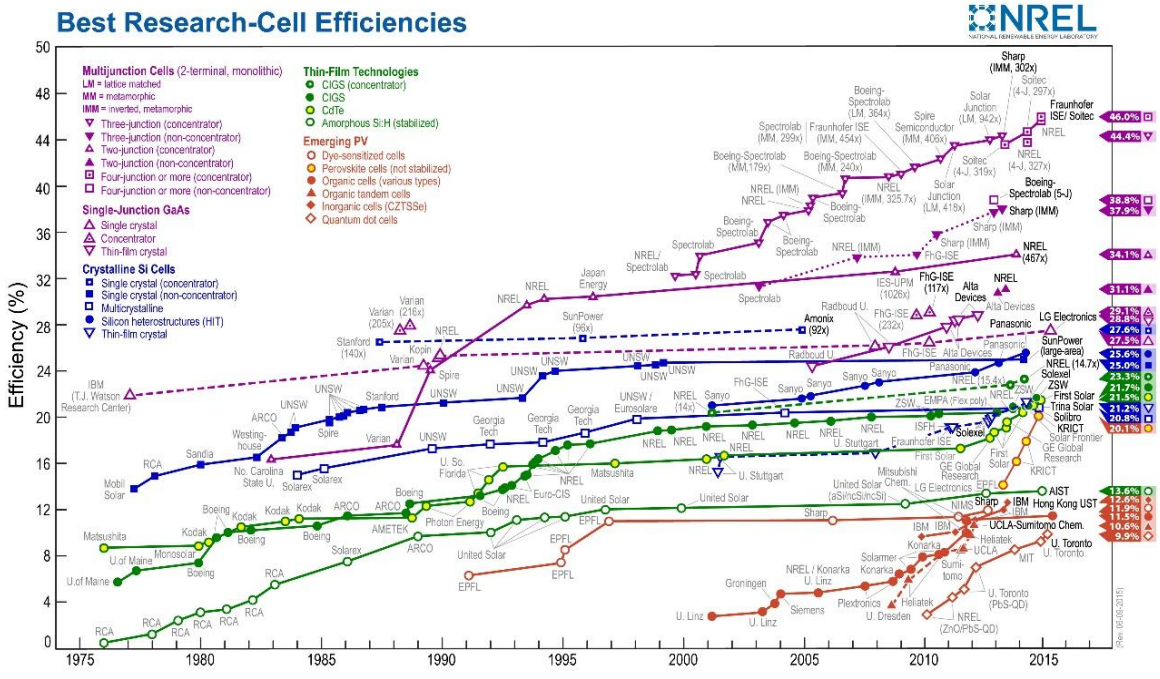

Figure 1.11 A graph representing the best research solar cell efficiencies

Chapter 2: Carbon

2.1. Carbon hybridisation:

Carbon is a non-metal element of the 4th periodic table group. It has four valance electrons which are capable of forming four covalent chemical bonds. The electronic structure o this atom in the ground state is: $1s^2$, $2s^2$, $2p_x^1$, sp_y^1. In order for the carbon atom to form four covalent bonds, four unpaired electrons are needed. These unpaired electrons are made available when one electron is transferred from the 2s the $2p_z$ orbital creating the electronic structure: $1s^2$, $2s^1$, $2p_x^1$, $2p_y^1$, $2p_z^1$.

The carbon atom 2s and 2p orbitals hybridise forming sp^x hybridised orbitals.

2.2. Allotropes of carbon:

Due to its valency, carbon is capable of forming various allotropes such as graphite, diamond, graphene and fullerene. The last allotrope mention is of great importance within this diploma thesis and in OPV development in general.

a) Graphite:

In graphite, multiple carbon atoms are linked with each other via sp^2 hybridisation. Each carbon atom forms a single bond with three neighbouring carbon atoms creating a two-dimensional hexagonal structure. These structures are stacked on top of each other and each sheet is known as ***graphene***.

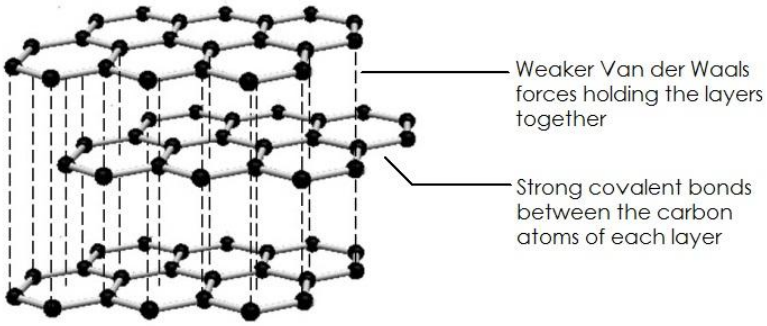

Figure 2.1 Carbon atom structure in graphite

Multiple graphene sheets are held together via Van der Waals forces forming the layered, planar structure of graphite. Graphite, unlike a diamond, is an electrical conducting material due to the dislocation of the π-electrons. The three sp2 electrons of each carbon atom is used in three σ-bonds with neighbouring carbon atoms. The fourth electron is located in the p_z orbital. Each p_z orbital is perpendicular to the plane defined by the σ-bonds and overlaps sideways with the p_z orbital of the neighbouring atoms, thus creating a system of π-molecular orbitals.

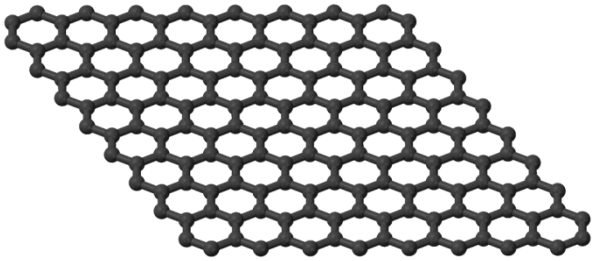

Figure 2.2 Carbon atom structure in graphene-the individual layer found in graphite.

b) Graphene: As mentioned previously, graphene is a planar allotropic structure of carbon. It is a 2D material with high crystallinity, a thickness of only one carbon atom and is a crucial component of other allotropic carbon structures. A structure of over 10 stacked layers of graphene is considered a 3D material (graphite). Graphene can also be enfolded to form ***fullerene***, a 0D material or bended to form carbon nanotubes, a 1D material. All these structures are shown in Figure 2.3.

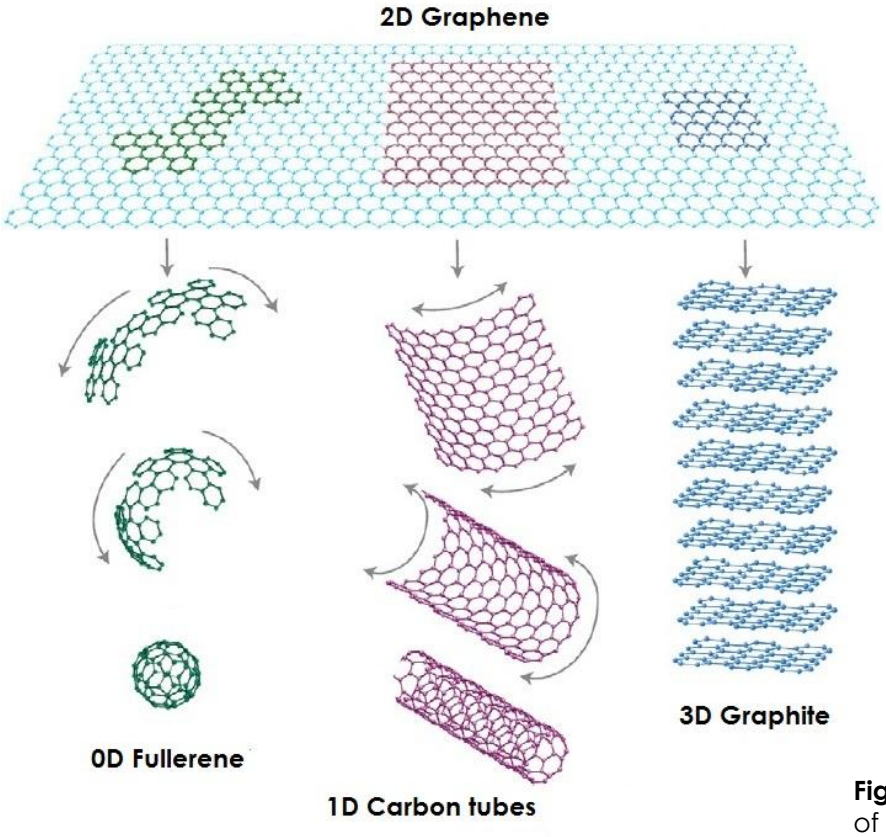

Figure 2.3 Allotropic structures of carbon

c) Fullerene:

In 1966 David Jones suggested that if pentagonal ring were to be inserted between the hexagonal rings of graphene, then the material would bend resulting in a closed, spherical structure[18]. This theory was proven correct in 1985 when Harold W. Kroto, Robert F. Curl and Richard E. Smalley discovered

a new allotrope of carbon, in which the atoms are arranged in closed shells. The new form, which consisted of 60 carbon atoms, was found to have the structure of a truncated icosahedron, and was named Buckminsterfullerene (Bucky ball).

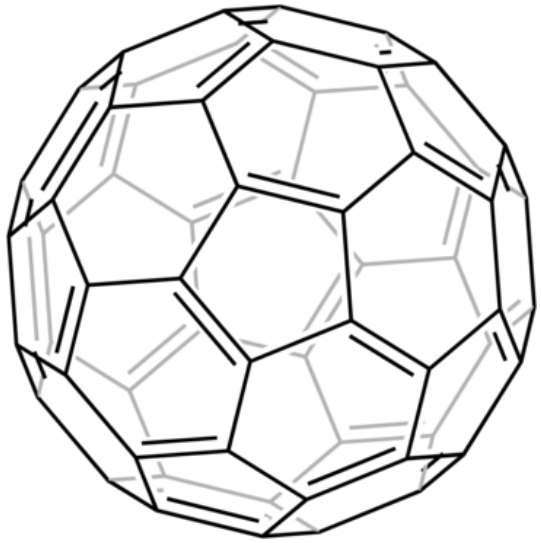

Figure 2.4 Structure of Buckminsterfullerene

The definition of fullerenes typically refers to a compound which consists exclusively of an even number of carbon atoms that form a polycyclic, cage shaped structure of 12 five-membered rings and 20 six-membered rings. Each carbon atom is connected to three neighbouring carbon atoms creating a uniform spherical grid which consists of alternating single and double bonds.

In OPVs, fullerenes are used as electron acceptors in the active layer blend. Fullerenes have a high electron affinity. This property lead to their use as electron transfer complexes alongside weak electron donors, such as conjugated polymers, in organic photovoltaics. The unique physical and electronic properties of fullerenes can be enhanced with the insertion of additional groups via chemical tuning. The specific fullerene derivative used in the experiments at hand will be described in further detail in Chapter 3 .

2.3. Conjugated polymers:

A polymer is a macromolecule which consists of repeating identical subunits (monomers). Until the 1970's all polymers which had been discovered were insulators (e.g. polyethylene (PE)) (Figure 2.5). In polyethylene (PE), the carbon atoms along the main polymer chain are connected via single bonds. The outer shell electrons show sp^3 hybridiasation and are arranged in a tetrahedral fashion. The saturation of the bonds in PE explains the very low electric conductivity. The electrons are incapable of movement, making this compound an insulator.

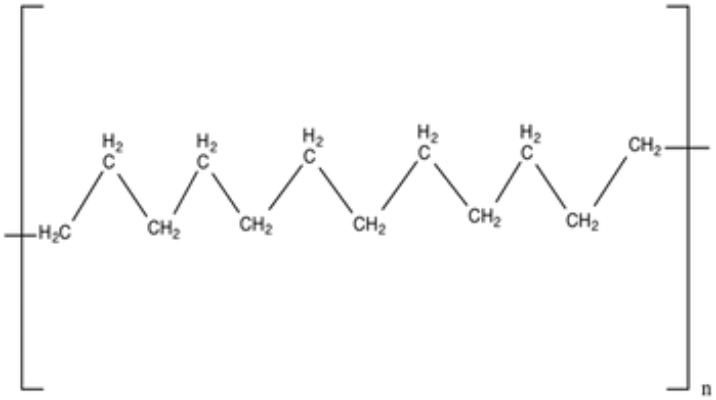

Figure 2.5 Polyethylene chain

Contrary to PE, the bonds in conjugated polymers are unsaturated. More specifically, they possess a system of alternating single and double bonds along the polymer chain. This is the origin of the conductivity and semi-conductivity behavior in conjugated polymers and comes as a result of chemical bonding behavior of the carbon atoms.

Each carbon atom in the ground state has an electron configuration of: two electrons with opposite spin in the 2s orbital and two lone electrons in the 2p orbital. Carbon can form two types of bonds: the σ-bond and the π-bond. A σ-bond is formed when the hybridised orbitals of adjacent carbon atoms, which are oriented along the polymer chain, overlap. Carbon atoms form three sp^2 hybridised orbitals ($2p_x$, $2p_y$, 2s) which are co-planar and at an angle of 120^o with each other, as shown in Figure 2.6.

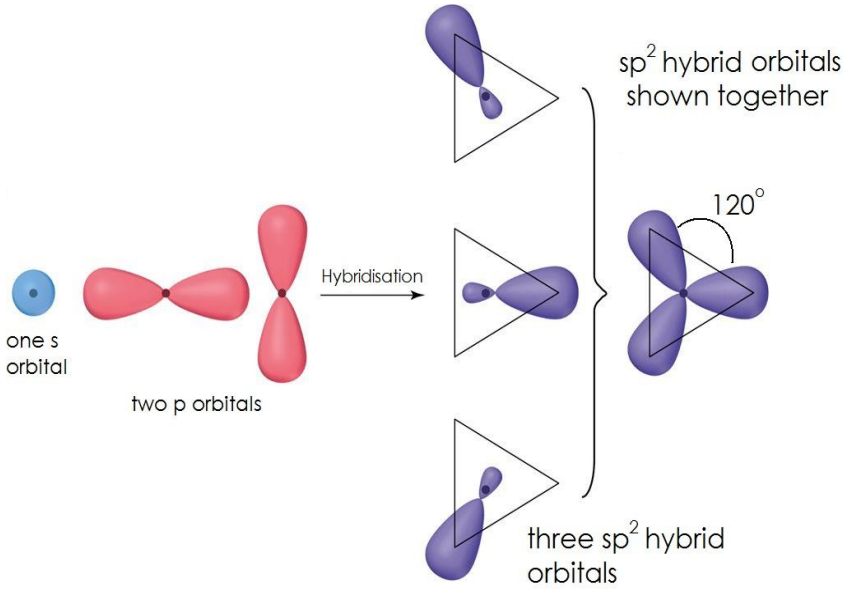

Figure 2.6 sp^2 hybridised orbitals of the carbon atom

An example of a conjugated polymer is polyethyne (or polyacetylene, PAc)(Figure 2.7). In PAc, the three sp^2 hybridised orbitals in each carbon atom

are occupied by three lone electrons and therefore form three σ-bonds: two with neighbouring carbon atoms and one with a hydrogen atom. The fourth electron is located in the out of plane p_z orbital.

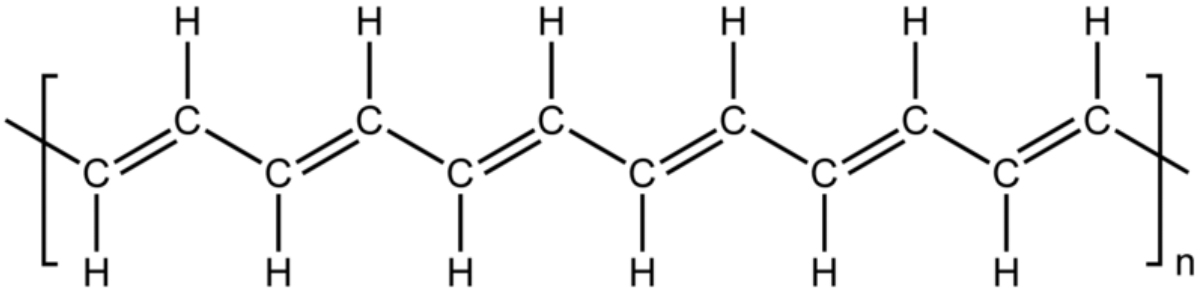

Figure 2.7 Alternating single and double bonds along the polyacetylene chain.

This orbital overlaps sideways with neighbouring p_z orbitals forming π-bonds which are perpendicular to the polymer chain. The electron inhabiting in these orbitals are delocalised along the polymer backbone, resulting in the conductive properties observed in conjugated polymers. The overlapping p-orbitals create a system of delocalised π-electrons, which can result in interesting and useful optical and electronic properties. Furthermore, the π-electrons can be moved easier from one bond to the other, which makes conjugated polymers one-dimensional (1-D) semiconductors.

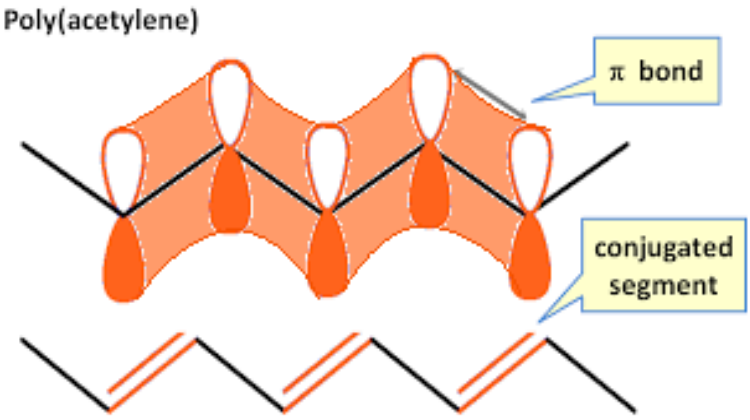

Figure 2.8 Delocalised electron density created by overlapping p_z orbitals in polyacetylene.

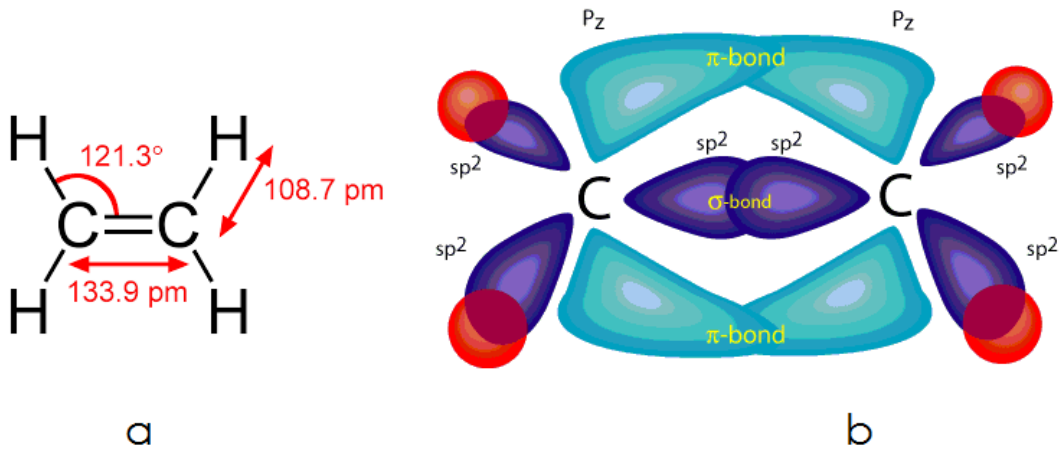

Figure 2.9 Orbitals and σ- and π-bonds in ethylene

The overlap of p_z orbitals results in two molecular orbitals (MO) – a bonding π-orbital which is the Highest Occupied Molecular Orbital (HOMO) and an antibonding π*-orbital which is the Lowest Unoccupied Molecular Orbital (LUMO). A schematic of the formation of these bonds is shown in Figure 2.10.

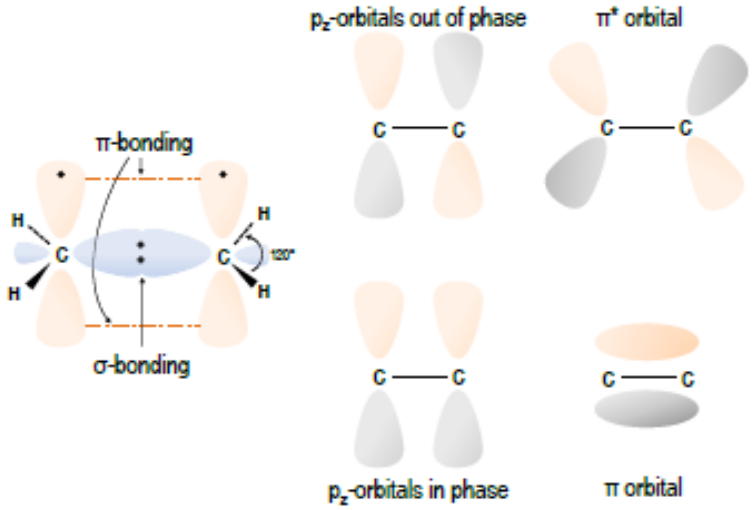

Figure 2 Overlap of p_z orbitals to give π and π* orbital (HOMO and LUMO respectively) in ethylene.

The π-orbital is equivalent to the valance band and the π*-orbital is equivalent to the conduction band. The energy difference between the HOMO and the LUMO is called the band gap (E_g) of the organic material and it determines its optical and electrical properties. The overlapping between two $2p_z$ orbitals is significantly smaller in comparison to that of the σ-bonds.

Therefore, the separation energy of the bonding and anti-bonding π-orbitals is much smaller (between 1-3 eV) [19].

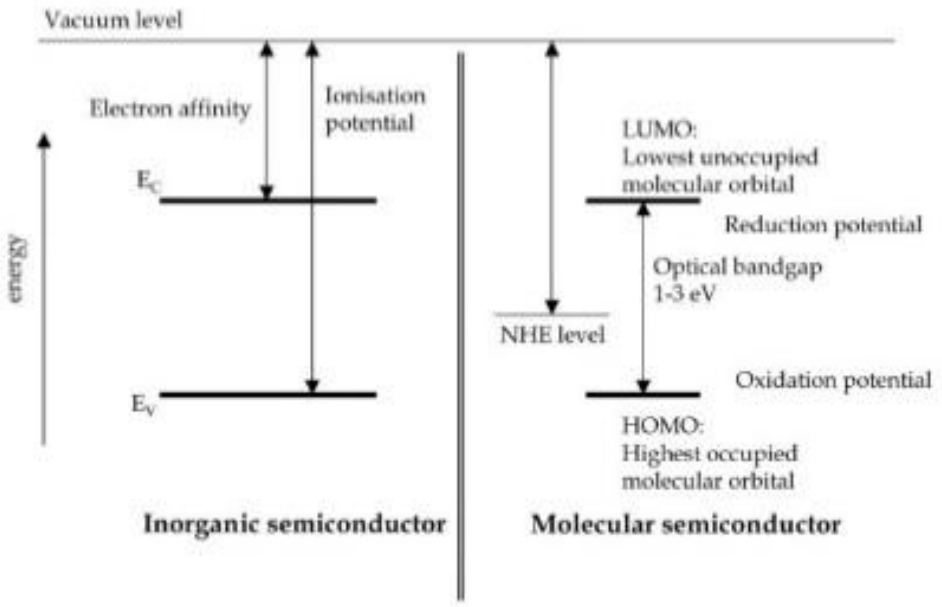

Figure 2.11 Energy levels in inorganic and organic semiconductors.

Chapter 3: Materials in Organic Photovoltaic Cells

The present diploma thesis presents a project in which bulk-heterojunction OPVs were fabricated and measured. Figure ... shows the general structure and the layers of a Bulk Hetero-Junction (BHJ) OPV. In this chapter, the role of each layer, as well as the materials used are described in detail.

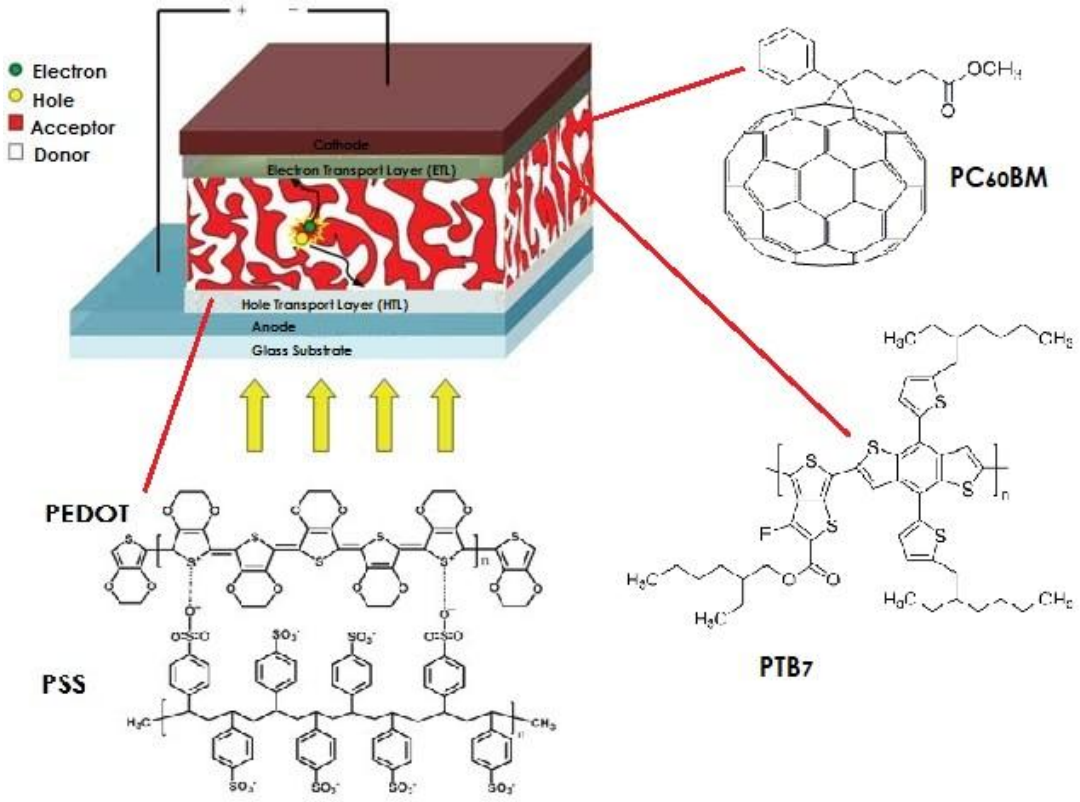

Figure 3.1 General layer structure of a Bulk Hetero-Junction (BHJ) OPV and the materials utilized for each layer.

3.1. Anode/Positive Electrode:

The anode is the electrode where the holes are collected. The material used as the positive electrode in this project was Indium Tin Oxide (ITO, In_2O_3:Sn). ITO is a Transparent Conductive Oxide (TCO). TCOs are essentially doped metal oxides. They are wide band-gap semiconductors that have a relatively high concentration of free electrons in its conduction band. These materials uniquely combine optical and photoelectrical properties (superior stability, high transparency in the visible range and high electrical conductivity) and are therefore widely used as electrodes in a large variety of optoelectronic

devices. Their typical resistivity values are on the order of 100–200 μΩ cm, which is 50–100 times larger than that of Ag or Cu. Nevertheless, such a level of resistivity is low enough to realize 10 Ω/sq when they are 100–200 nm thick. Due to their low absorption coefficient in the visible and NIR region, T of approx. 85–90% is readily achieved in such a thickness range. The relatively low roughness of ITO electrodes [25,51] has also been the reason for its popularity in OPVs[20].

Glass substrates (20x15x1.1 mm) coated with an ITO pattern were purchased by Luminescence Technology Corp. The ITO layer has a thickness of about 100nm, a surface resistance of ~20 Ω/ sq and work function of around 4.7 eV. A schematic representation of the ITO pattern is shown in Figure 3.2.

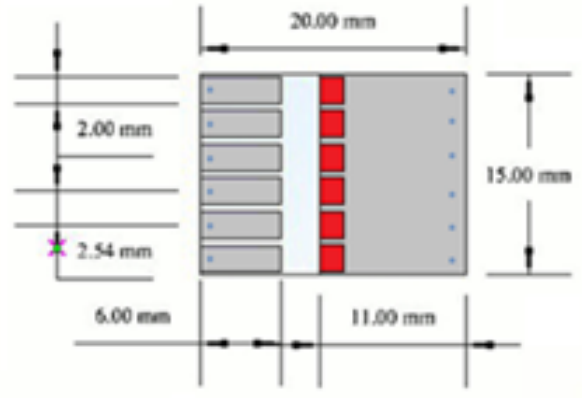

Figure 3.2 Physical dimensions of the patterned ITO glass.

Grey areas: ITO

Red areas: Active areas

Blue dots: Contacts

3.2. Hole Transport Layer (HTL)/Electron Blocking Layer (EBL):

The hole transport layer is placed between the active layer and the positive electrode and it prevents electrons from travelling from the active layer to the positive electrode and as a result forcing the electrons to travel in the correct direction to be collected at the negative electrode (cathode). If it weren't for the HTL, electrons from the electron donor in the active layer blend would be transferred to the ITO layer and would recombine with holes, resulting in charge losses and thus a reduced open circuit voltage (V_{OC}).

The EBL/HTL used in the fabrication of these devices was Poly(3,4-ethylenedioxythiophe ne)poly(styrene sulfonate) or PEDOT:PSS (Figure 3.3). PEDOT:PSS is a polymer mixture of two ionomers. One component in this mixture is made up of sodium polystyrene sulfonate (PSS) which is a sulfonated polystyrene. Part of the sulfonyl groups are deprotonated and carry a negative charge. The other component poly(3,4-ethylenedioxythiophene) or PEDOT is a conjugated polymer and carries

positive charges and is based on polythiophene. Sulfonate groups withdraw electrons from the PEDOT backbone and then transform the chain electronic state from neutral to polycationic. The PSS serve then the dual purpose of oxidizing PEDOT moieties and stabilizing in aqueous media the otherwise insoluble polymer. Together the charged macromolecules form a macromolecular salt (PEDOT:PSS) that is generally applied dispersed in water (H_2O solved). These two materials (PEDOT and PSS) exhibit high transparency in light of wavelength in the region 350-900 nm. This material is used as a transparent, conductive polymer with high ductility in different applications. Furthermore, it reduces the roughness of the ITO layer and optimises the electric contact with the active layer. Additionally, increases the work function of the positive electrode from 4.7-4.9 eV (that fluctuates the work function of ITO) to 5-5.1 eV, helping to better charge transport and charge collection.

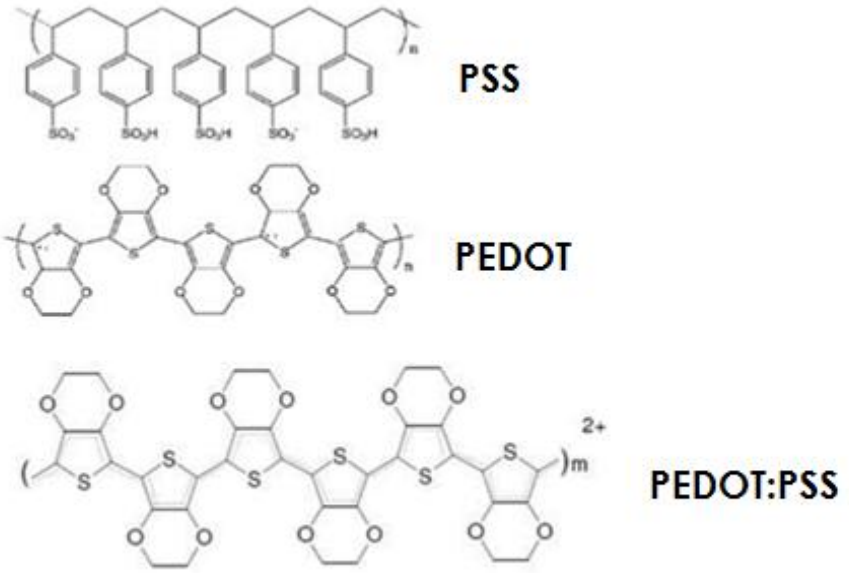

Figure 3.3 Chemical structures of PEDOT and PSS polymers and the mixture they form.

Due to its unusual properties, PEDOT:PSS has been intensively studied and it has been revealed that subtle changes in the molecule conformation could lead to dramatic alteration of its electronic properties.

In a series of experiments during this project, a two-step treatment method was adopted in order to investigate the effects of the addition of organic solvents, namely dimethyl sulfoxide (DMSO) and tetrafluoroethylene-

perfluoro-3,6-dioxa-4-methyl-7-octenesulfonic acid copolymer (PFI or Nafion™) to the PEDOT:PSS. This treatment method has been reported to simultaneously improve the performance of PEDOT:PSS. This treatment was designed to improve the work function and conductivity of PEDOT:PSS for further extracting hole from the BHJ layer, as well as to enhance the transmittance of PEDOT:PSS for minimizing the optical losses[21] It has been reported that the conductivity of PEDOT:PSS could be changed by doping different organic solvents, such as glycerol, dimethyl sulfoxide (DMSO) and Ethylene glycol (EG)[22][23]. While comparing to pristine PEDOT:PSS, solvent treated PEDOT:PSS typically shows decreased work function values,[24], [25],[26] which could increase the charge extraction barrier. Lee reported that the addition of tetrafluoroethylene-perfluoro-3,6-dioxa-4-methyl-7-octene-sulfonic acid copolymer (PFI) increased the work function of PEDOT:PSS.

Firstly, tetrafluoroethylene-*perfluoro-3,6-dioxa-4-methyl-7-octenesulfonic acid copolymer (PFI or Nafion™),* a perfluorinated ionomer was added to the PEDOT:PSS and secondly it was treated with a dimethyl sulfoxide (DMSO) bath. The way in which the two-step treatment took place is described in the experimental section in Chapter 5.

3.3. Tetrafluoroethylene-perfluoro-3, 6-dioxa-4-methyl-7-octenesulfonic acid copolymer (PFI) additive:

PFI is an anionic fluorinated material and its addition to the PEDOT:PSS hole transport layer, allows us to investigate the effect of fluorination on the electronic properties of PEDOT:PSS and in the performance of OPV devices.

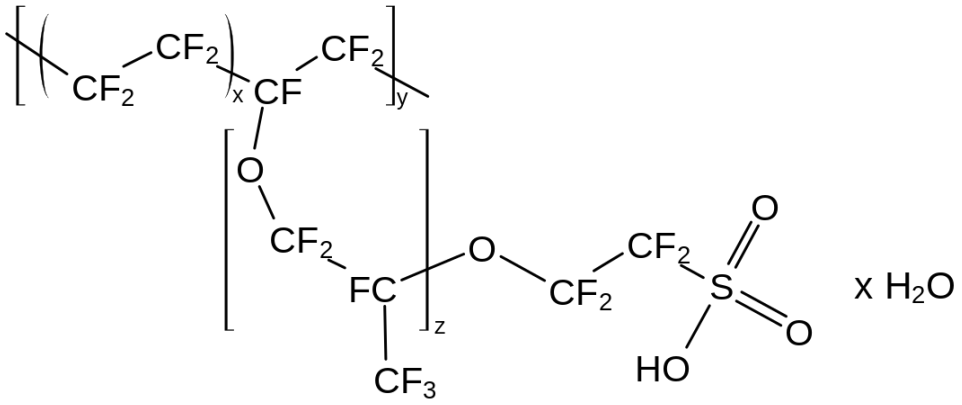

Figure 3.4 Chemical structure of PFI.

Fluorine is the most electronegative element with a Pauling electronegativity of 4.0.

The fluorination effect on the solar cell performance has recently been investigated systematically. Blending fluorinated molecules in PEDOT:PSS HTLs induces charge transfers which impact on both charge extraction and photogeneration[27].

The addition of PFI to the PEDOT:PSS solution as a means of fluorination has been shown to result in a changed conductivity and morphology[27][21], and therefore device performance. The enhanced device performance and photovoltaic characteristics are investigated in this experiment and discussed in Chapter 6.

3.4. Treatment with dimethyl sulfoxide (DMSO):

The conductivity of PEDOT:PSS can be increased by up to two or three orders of magnitude by adding high-boiling point and/or polar compounds such as dimethyl sulfoxide (DMSO), due to the phase separation of each PEDOT-rich region and PSS-rich region.
The underlying mechanisms on conductivity improvement of PEDOT:PSS can be summarized as follows[28]:

a) The excess insulator PSS is washed away from the film surface. Jonsson et al. proposed that PPS molecules are washed away by the organic solvent from the surface region of the PEDOT:PSS film, resulting in higher PEDOT:PSS ratio on the surface of the film[29]. It can be considered that the diameters of the primary particles would decrease by the wash-effect, resulting in thinner film if it is the monolayer of the primary particles. It is considerable that the PEDOT:PSS thin films that are fluxed with an organic solvent, such as DMSO, may consist of clusters (aggregates) of primary particles with decreased diameters by the wash-effect[30] .With the removal of the PSS capping layer, the conductivity of PEDOT:PSS is increased.

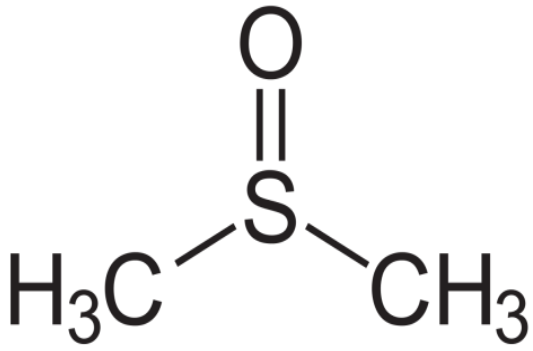

Figure 3.5 Chemical structure of dimethyl sulfoxide.

b) DMSO-fluxing treatment induces strong screening effect between counter ions and charge carriers, which reduces the coulombic interaction between positively charged PEDOT and negatively charged PSS dopants.

c) The thickness of the HTL decreases when fluxed with DMSO which is also conducive to the increase of conductivity.

In general, the higher the conductivity, the easier the charge collection is.

Although there exists a substantial amount of literature related to explaining the improvement in conductivity of PEDOT:PSS via DMSO treatment, the mechanism with which this is achieved is still widely debated. However, as mentioned above, it has been generally accounted to screening effects between PEDOT and PSS chains due to the polar solvent enhanced charge mobility due to an improved interchain packing and thinner PSS barriers. In addition, the creation of PEDOT-rich regions after immersion in a polar organic solvent such as DSMO is another proposed mechanism[31]. Post-treatment of a PEDOT:PSS film has been shown to turn the film insoluble and improve the conductivity by removing PSS. The removal of PSS creates a more homogeneous and conductive surface. Adding DMSO to the PEDOT:PSS solution is thought to cause the PEDOT and PSS to rearrange into a more favourable conformation within the film[32].

3.5. Photo-active Layer:

In BHJ OPVs the active layer consists of a blend of an electron donor and electron acceptor. This is the key difference between a BHJ organic solar cell and other OPV structures. The devices fabricated used a mixture of a fullerene as the electron acceptor and a conjugated polymer as the electron donor.

3.5.1. Electron Donor:

In semiconductor physics, a donor is a dopant atom which, when added to a semiconductor can form an n-type region as the number of electrons in the conduction band increase. It is essentially an impurity atom in a semiconductor which can contribute or donate one or more conduction electrons to the crystal by becoming ionized and positively charged.

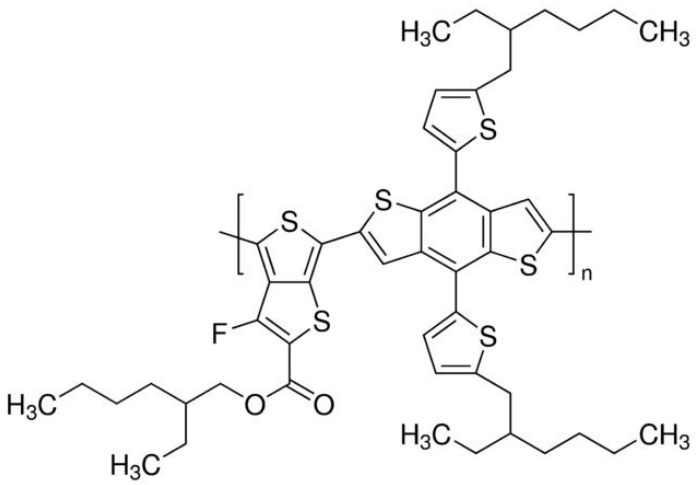

Figure 3.6 Chemical structure of PTB_7.

For example, an atom of column 5 of the periodic table substituting for a regular atom of a germanium (Ge) or silicon (Si) crystal is a donor because it has one or more valence electrons which can be detached and added to the conduction band of the crystal.

The electron donor used was *Poly({4,8-bis[(2-ethylhexyl)oxy]benzo[1,2-b:4,5-b'] dithiophene-2,6-diyl}{3-fluoro-2-[(2-ethylhexyl)carbonyl]thieno [3,4-b]thiophenediyl})*or ***PTB_7*** (Figure 3.6) **.**

3.5.2. <u>Electron Acceptor:</u>

Fullerenes are often utilized as electron acceptors in OSCs due to their relatively high electron affinity and charge carrier mobility. The material used as the electron acceptor in the active layer blend was the fullerene derivative of C_{60} *[6,6]-phenyl-C61-butyric acid methyl ester ($PC_{60}BM$)*(Figure 3.7).

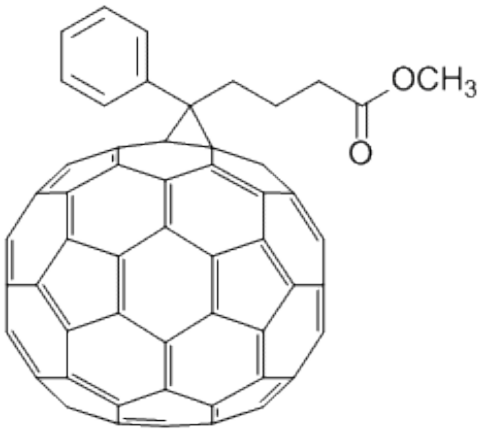

Figure 3.7 Chemical structure of $PC_{60}BM$.

Fullerene C_{60} has well-symmetric structure and exhibits good electron mobility, and as known, one molecule of C_{60} can receive four electrons. Therefore, C_{60} and its derivatives can be used as electron acceptor materials. Although, C_{60} can be dissolved in Chlorobenzene (CB) and Dichlorobenzene (DCB), it exhibits very limited solubility in most of the commonly used organic solvents. In order to improve its solubility and also to avoid severe phase separation of Donor/Acceptor blend, [6,6]-phenyl-C61-butyric acid methyl ester ($PC_{60}BM$) was applied in OPVs. $PC_{60}BM$ is crystalline dark-brown powder, and possesses good solubility in common organic solvents such as Chloroform, Toluene and o-Dichlorobenzene (ODCB). In the past decade, $PC_{60}BM$ and its corresponding C_{70} derivative ($PC_{70}BM$, Figure 3.8) have been dominantly used as acceptors in OPVs. In comparison with $PC_{60}BM$, $PC_{70}BM$ possesses stronger absorption in visible range, and hence it attracted much interest recently. However, C_{70} is much expensive than that of C_{60} due to its tedious purification process, which limits its application.

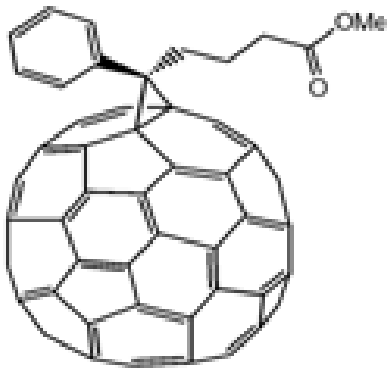

$PC_{70}BM$

Figure 3.8 Chemical structure of $PC_{70}BM$.

Both the two materials show strong absorption at ultraviolet region, from 200 to 400 nm, but $PC_{70}BM$ shows stronger absorption in visible region compared to $PC_{60}BM$. The electrochemical properties and energy level of the fullerene derivatives is very important for OPVs. As it is shown in Figure 3.9 , $PC_{60}BM$ has a 4.2 eV LUMO and 6.0 eV HOMO level and $PC_{70}BM$ 4.2 eV and 6.1 eV respectively. The open-circuit voltage (Voc) of OPVs is determined by the difference between the LUMO energy level of the fullerene acceptors and the HOMO energy level of the polymer donors. Therefore, the LUMO energy level of the fullerene derivatives is a key parameter for the application of an acceptor to match with a polymer donor.

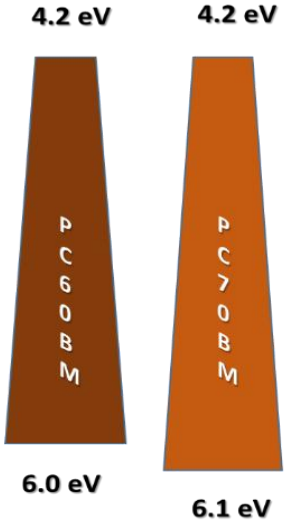

Even though the HOMO and LUMO energy levels of $PC_{70}BM$ make it a better electron acceptor than $PC_{60}BM$, the latter was preferred in the fabrication of the solar cell devices in this project for economic reasons. Never the less, $PC_{60}BM$ is a sufficient electron acceptor with a strong absorption in the UV region.

Figure 3.9 Energy levels (HOMO-LUMO) of $PC_{60}BM$ $PC_{70}BM$.

3.6. Interlayers:

One of the key points for a good performing OSC is undoubtedly represented by the quality of charge collection at the electrodes. Charge carriers, formed in the active layer upon exposure to sunlight, need to be effectively collected by the respective electrodes (holes at the anode and electrons at the cathode), in order to be exploited.

The main obstacle is represented by the non-ideal nature (i.e., non-ohmic) of the contacts between the active layer and the electrodes. In real devices, barriers for charge extraction are present at one or both sides of the active layer, causing a diminished V_{OC} and affecting FF due to charge accumulation at the electrode–active layer interface. The poor energy-level alignment is a common feature of non-optimized OSCs, originating from several sources (i.e., choice of the electrode material, non-conformal adhesion between adjacent layers, chemical reactions occurring at the electrode–active layer interface, etc.) and is responsible for non-optimal performance. The use of suitable interlayers is an effective approach to improve energy level alignment and avoid these aforementioned complications[33].

It is preferable for the cathode interface to have a low work function contact for efficient electron extraction. While Al and Ag are the most common electrode materials used in organic solar cells the thermal evaporation process which is used to apply the metal frequently alters the quality of the metal/organic interface. The reactive hot metal atoms can lead to chemical interaction at the interface and diffusion into the organic layer[34]. Antoniadis suggested that the instability of the Al

electrode is related to the Al–C bond formation, which interrupts the p-conjugated system. In order to prevent this problem from occurring, other low work function metals such as Ca, Mg, and Ba, are often employed to protect the metal/organic interface, while being capped by the Al or Ag electrode. Inserting Ca between the Al electrode and the polymer forms an Ohmic contact that results in a high fill factor (FF). The thin n-doped layer induced by Ca deposition pins the surface energy level at the polymer/metal interface, which facilitates the charge transport[35]. Ca reacts with water at room temperature, while being relatively inert to molecular oxygen[36] . Nonetheless, the instabilities of Ca and Mg in ambient atmosphere require combining with metals with a low permeation rate to moisture such as Al and Ag to form effective cathodes.

3.7. Cathode/Negative Electrode:

In conventional devices, Aluminum (Al) is usually used as the metallic cathode because it matches with ITO Anode as it has a lower (absolute value) Work Function (WF). However, in the devices fabricated in this experiment, Silver (Ag) a high work function metal-about 4.26 eV-was used as the cathode. The method utilized to apply the metal cathode was Vacuum Thermal Evaporation (VTE), which will be further analysed in Chapter 5.

Chapter 4: Structure and General Operating Principals of Organic Solar Cell

4.1. Device structure:

There are two main device structures utilised for the fabrication of BHJ organic solar cells: conventional and inverted. These two structures differ in the order in which the layers are deposited onto the substrate.

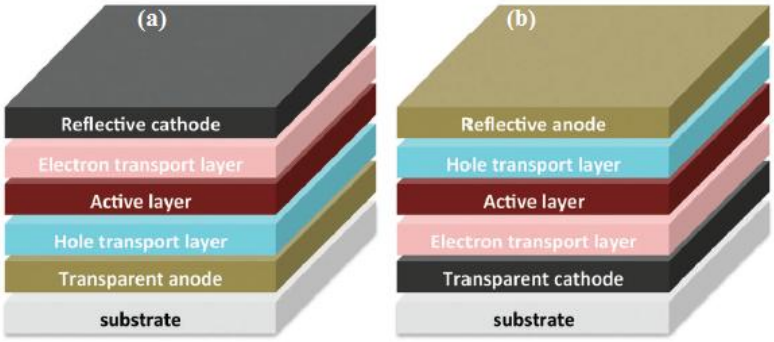

Figure4.1 a) Conventional BHJ device structure b) Inverted BHJ device structure.

In the conventional configuration, a transparent substrate (glass or plastic) is coated with a transparent conductor that serves as the anode. The anodes role is firstly to allow light to pass through and secondly to collect holes which are generated in the active layer. As mentioned in Chapter 2, the anode material used was ITO (**I**ndium **T**in **O**xide) which is a TCO (**T**ransparent **C**onducting **O**xide). A hole transport layer (HTL) is deposited in between the anode and the active layer. In our case PEDOT:PSS was used. This layer not only helps the holes reach their destination at the anode but also prevents electrons from reaching the anode. This layer essentially serves as a hole conducting layer and an exciton blocker. It improves the morphology of the ITO surface, seals the active layer from oxygen, and prevents the anode material from diffusing into the active layer, which can lead to trap sites.

The light absorbing photoactive layer containing the donor and acceptor material is sandwiched between two electrodes. In our case the active layer is the polymer-fullerene blend PTB_7-$PC_{60}BM$ in which the polymer is the donor and the fullerene is the acceptor. In between the active layer and the cathode there is an electron transport layer (ETL), in our case Calcium (Ca), which helps electron reach the cathode while simultaneously blocking holes from reaching this layer. The last layer to be deposited is the negative electrode (a metal cathode), which in our case is Silver (Ag). The function of

the cathode is to collect the electrons generated in the active layer of the device.

Often, the low-work function (WF) metals used for the electron-transport layer (ETL) in this configuration are highly reactive and contribute to device degradation (as PEDOT:PSS), so inverted geometries (Fig. 3.2 b) are sometimes employed where the electrodes are switched and different buffer layers are applied. Inverted architectures are also generally more compatible with roll-to-roll processing, another substrate deposition method.

4.2. Operating principles of polymer OPVs:

The operation mechanism of OPVs in which solar energy is converted to electric energy is based on five basic steps.

1. Creation of a singlet exciton from the absorption of a suitable energy photon.

2. Diffusion of the exciton at the donor-acceptor interface.

3. Disassociation of exciton-Transfer of electron to the electronegative acceptor material.

4. Separation of the polaronic electron-hole pair.

5. Charge collection at the electrodes.

4.3. Exciton generation, Light-induced charge transfer:

A key difference between inorganic and organic photovoltaic cells is the nature of the excited state. In inorganic semiconductors the absorption of a photon at room temperature results in the direct generation of free electrons and holes. These charge carriers may diffuse or travel toward the respective electrodes. In organic semiconductors, however, the absorption of a photon results in the formation of an exciton-a bound state of an excited electron and the associated holes which are bound by electrostatic Coulomb force and move as a uniform particle. This is a result of the low dielectric constant ($n \approx 3$) in semiconducting polymer materials. The coulombic forces of attraction

between electrons and holes are very high[37]. This implies that unlike inorganic semiconductors, in which photo excitation generally forms a free electron and hole excited states in semiconducting polymers form bound electron-hole pairs. Once an exciton is formed it can dissipate for a distance of 5-35nm[38]. Its de-excitation then follows either with or without radiation emission. Singlet excitons take a few ps to diffuse emit fluorescence and triplet excitons take a few ns to diffuse emitting phosphorescence. For excitons to be of use in photovoltaic cells they must dissociate into electrons and holes before diffusion can take place.

In BHJ OPVs, photons travel through the transparent electrode (ITO) and are absorbed by the donor-acceptor blend (PTB_7:$PC_{70}BM$) in the photoactive layer. Excitons are formed in the acceptor material of the active layer. They then travel to the donor-acceptor interface where they diffuse freeing electrons and holes. The electrons travel from the donor to the acceptor material/ More specifically, a LUMO electron from the donor material is transferred to a LUMO of the acceptor leaving behind a hole in the HOMO of the donor.

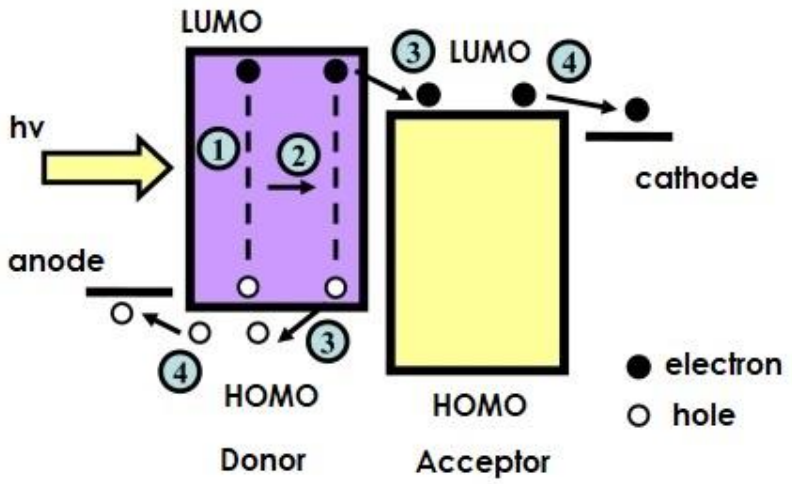

Figure 4.2 (1) Photon absorption and exciton generation; (2) exciton diffusion; (3) exciton dissociation; (4) carriers collection.

A driving force is required to overcome this excitonic binding energy (Coulomb bonding) so that free charge carriers can be produced and transported throughout the device. The force required to overcome the exciton binding energy (exciton dissociation) is provided by the energy level offset of the LUMO of the donor and the LUMO of the acceptor material (higher electron affinity of acceptor). In order to dissociate

excitons formed in the acceptor material, the energy offset of the highest occupied molecular orbital (HOMO) of the acceptor and the HOMO of the donor material is required. This energy offset used to dissociate excitons is illustrated as ΔE_{GS} Fig. 3.8, which is the ground state energy offset. Excitonic dissociation due to these energy offsets occurs at the interface between the donor and acceptor phase, therefore, the arrangement of the two materials in the active layer is crucial for the successful operation of the device

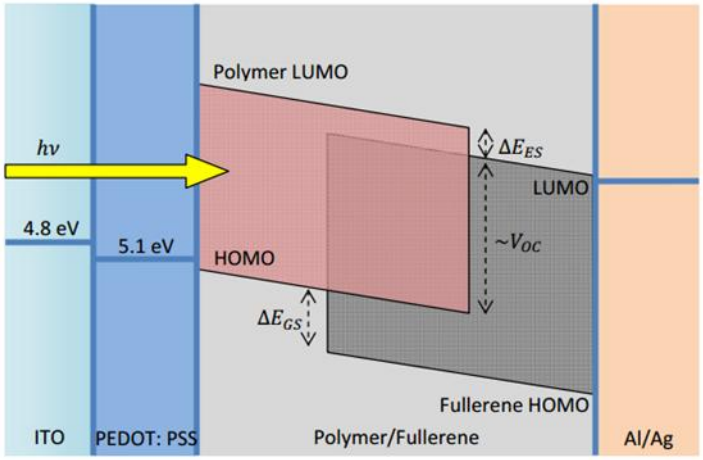

Figure 4.3 Energy band diagram of donor-acceptor materials in BHJ OPVs.

Exciton diffusion in organic semiconductors is crucial to the performance of organic solar cells. The lifetime of the singlet exciton in most conjugated polymer films is short; typically less than 1 ns, the diffusion lengths are limited to less than 20 nm[39]. The BHJ structure is a successful approach in order to significantly increase the interfacial area. A device with a large dispersion of interfaces throughout the photoactive layer requires smaller exciton diffusion distances, and thus, a larger exciton dissociation yield is achieved. There exists a trade-off between increasing interfacial area via the intimate dispersion of phases and the creation of efficient conductive pathways through which free electrons and holes may be transported. The arrangement of donor and acceptor phase is thus crucial to device performance.

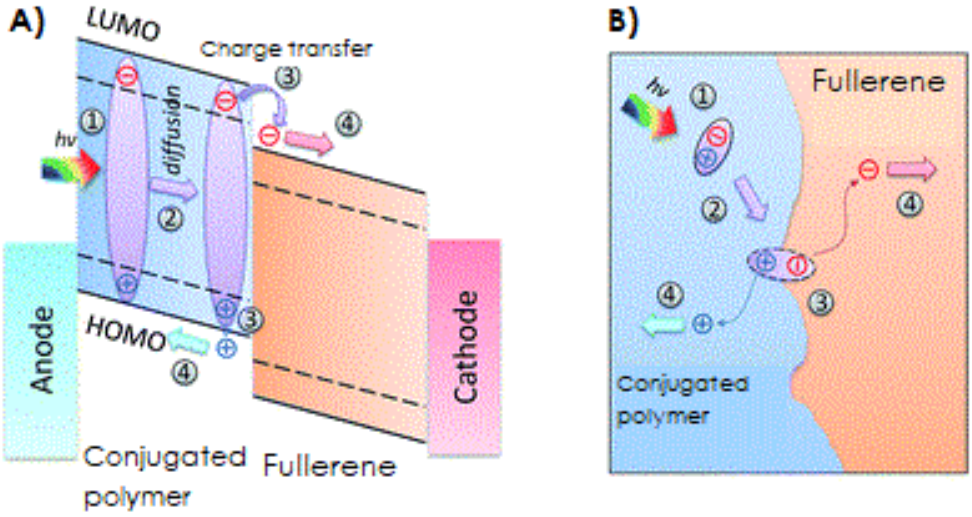

Figure 4.4 A) The diffusion of the exciton in the conjugated polymer and the transfer of the independent charge carriers through the respective layers. B) The electron is transferred through the fullerene to be collected at the cathode, while the respective hole travels through the conjugated polymer layer toward the anode.

4.4. Device characterisation-Parameters:

The standard parameters that are calculated after the experimental procedure are the short circuit current (J_{SC}), the open circuit voltage (V_{OC}), the fill factor (FF), of course the power conversion efficiency (PCE), all of which are presented in detail below. For the purposes of this experiment, the hole mobility (μ) in the HTL was also calculated. Lastly, the morphology of the reference PEDOT:PSS and the treated HTLs was investigated and compared using Atomic Force Microscopy (AFM).

4.4.1. Short circuit current density, Jsc:

The short circuit current (I_{sc}) is the current measured while the voltage has a value of zero. The value of I_{sc} is proportional to light intensity. This is because higher light intensity means more photons are absorbed and therefore more electrons are produced. Since the short circuit current I_{sc} is roughly proportional to the area of the solar cell, the short circuit current density is often used to compare solar cells.

$$\mathrm{Jsc} = \frac{\mathrm{Isc}}{\mathrm{A}}$$

Where A = Active Area (A.A). In our case, A=4mm^2.

When a charge is connected to the solar cell, the current decreases and a voltage develops as charge builds up at the terminals. The resulting current can be viewed as a superposition of the short circuit current, caused by the absorption of photons, and a *dark current*, which is caused by the potential built up over the load and flows in the opposite direction. As a solar cell contains a PN-junction, just as a diode, it may be treated as a diode. For an ideal diode, the dark current density is given by:

$$J_{dark(V)} = J_0[\exp\left(\frac{q*V}{n*K*R}\right) - 1] \quad (1.1)$$

Here, J_0 is a constant, q is the electron charge, V is the voltage between the terminals, n is the diode ideality factor, k is the Boltzmann constant and T the temperature.

$$J = J_{SC} - J_0[\exp\left(\frac{q*V}{n*K*R}\right) - 1] \quad (1.2)$$

The resulting current can be approximated as a superposition of the short circuit current and the dark current:

$$I_{dark} = I_L - I_s[\exp\left(\frac{V}{nKR}\right) - 1] \quad (1.3)$$

where, I_L is the electric current or the light-generated current and I_s is the saturation current of the diode.

4.4.2. <u>Open circuit voltage, Voc:</u>

The open-circuit voltage (V_{OC}) is the maximum voltage available from a solar cell and it occurs at zero current. The open-circuit voltage corresponds to the amount of forward bias on the solar cell due to the bias of the solar cell junction with the light-generated current.

In order to find an expression for the open circuit voltage, V_{oc}, we use equation (1.2) and set J = 0. This means that the two currents cancel each other out so that there is no current flowing, which is exactly the case in an open circuit. The resulting expression is:

$$V_{OC} = \frac{K_B * T}{q} \ln\left(\frac{J_{SC}}{J_0} + 1\right) \tag{1.4}$$

The built-in electric field separating the photogenerated electrons and holes can at most provide the built-in potential, V_{bi}. Hence, the built- in voltage gives the upper bound of the open circuit voltage. The effect of the parasitic series and shunt resistances, R_S and R_{SH} due to its bulk resistivity and presence of defects can included in the *Schockley* equation[40] as:

$$I = I_s \exp\left(\frac{q}{nKT}(V - IR_s)\right) - 1) + \frac{V - IR_s}{R_{SH}} - I_L \tag{1.5}$$

Figure 4.5 shows the equivalent circuit of p-n junction solar cell, in which the I-V curve of this circuit is described by the equation above. The circuit consists of the following three parts. A current source I_L that considers the light-generated current, a diode that accounts for the nonlinear voltage dependence and a shunt as well as a series resistor.

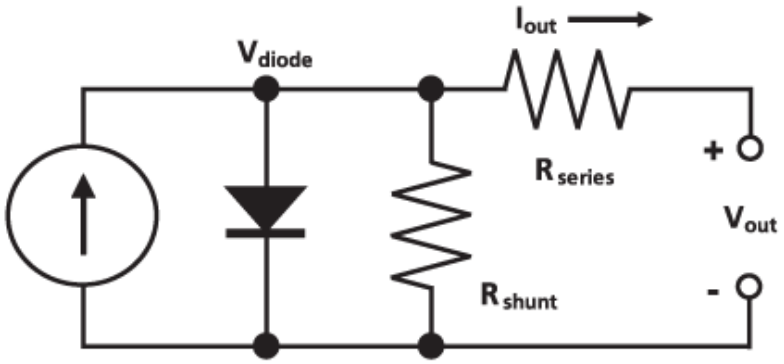

Figure 4.5 Equivalent circuit of a p-n junction solar cell[41].

The current source generates a current I_L up on illumination. I_L can be described as the number of free electron/hole pairs immediately after generation - before any recombination can take place. The series resistance R_S is due to the bulk resistance of the semiconductor material, the bulk resistance of the metallic contacts and the contact resistance between the metallic contacts and the semiconductor. The shunt resistance R_{SH} is caused by leakage across the p-n junction around the edge of the cell and in non-peripheral regions in the presence of defects and precipitates of foreign impurities in the junction region.

In conclusion, in the standard p-n junction solar cell, light absorption occurs via band gap excitation of electrons in the bulk of the semiconductor, charge separation in the internal electric field of the p-n junction and charge collection by transport of electrons and holes through the bulk of the semiconductor to the electrical contacts.

As we can see from Fig. 2.6 b) and Fig. 3.8, there is another way to find the V_{OC} from the difference of the $LUMO_{Acceptor}$ and $HOMO_{Donor}$:

$$V_{OC} = \frac{1}{e} * (LUMO_{ACCEPT} - HOMO_{DONOR}) - 0.3 \qquad (1.6)$$

Studies have shown that the value of V_{oc} depends largely on the relative energy levels of the donor and acceptor species that form the essential heterojunction.

4.4.3. I-V curve:

The graph seen in Figure 4.6 shows the current-voltage (I-V) characteristics of a typical PV cell operating under normal conditions. The power delivered by a solar cell is the product of current and voltage (I x V). If the multiplication is done, point for point, for all voltages from short-circuit to open-circuit conditions, the power curve above is obtained for a given radiation level.

With the solar cell open-circuited, that is not connected to any load, the current will be at its minimum (zero) and the voltage across the cell is at its maximum, known as the solar cells open circuit voltage, or V_{oc}. At the other extreme, when the solar cell is short circuited, that is the positive and negative leads connected together, the voltage across the cell is at its minimum (zero) but the current flowing out of the cell reaches its maximum, known as the solar cells short circuit current, or J_{sc}.

Then the span of the solar cell I-V characteristics curve ranges from the short circuit current (J_{sc}) at zero output volts, to zero current at the full open circuit voltage (V_{oc}). In other words, the maximum voltage available from a cell is at open circuit, and the maximum current at closed circuit. Of course, neither of these two conditions generates any electrical power, but there must be a point somewhere in between those two the solar cell generates maximum power.

However, there is one particular combination of current and voltage for which the power reaches its maximum value, at I_{mp} and V_{mp}, in other words, the point at which the cell generates maximum electrical power. This is the "maximum power point" or MPP and it is positioned near the bend in the I-V characteristics curve[42].

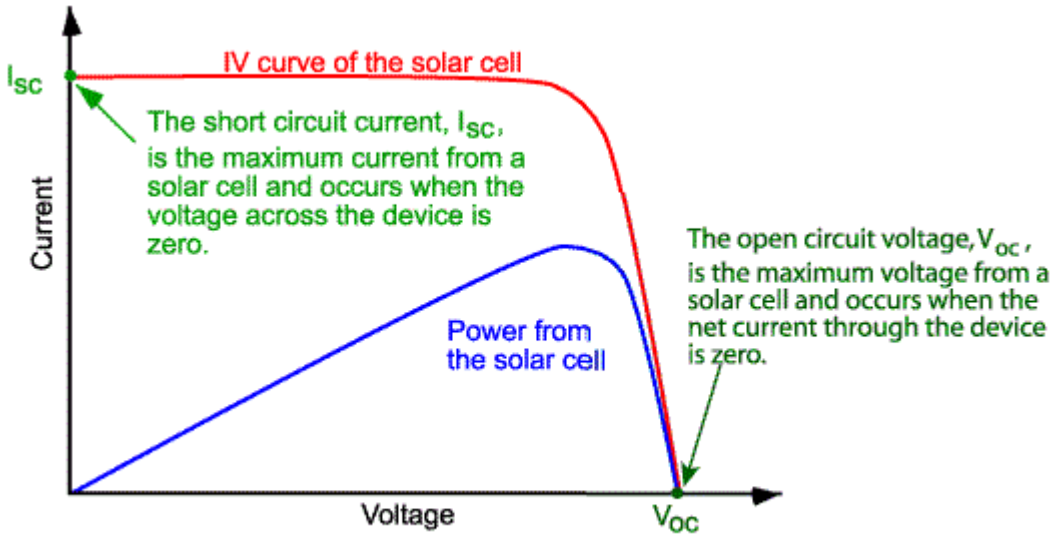

Figure 4.6 A typical I-V curve, where the Short circuit current and Open circuit voltage are shown.

4.4.4. Fill factor, FF:

The short-circuit current and the open-circuit voltage are the maximum current and voltage respectively from a solar cell. However, at both of these operating points, the power from the solar cell is zero. The "fill factor", more commonly known by its abbreviation "FF", is a parameter which, in conjunction with V_{oc} and I_{sc}, determines the maximum power from a solar cell. The FF is defined as the ratio of the maximum power from the solar cell to the product of V_{oc} and I_{sc}. Graphically, the FF is a measure of the "squareness" of the solar cell and is also the area of the largest rectangle which will fit in the IV curve. The FF is illustrated in Figure 4.7 below.

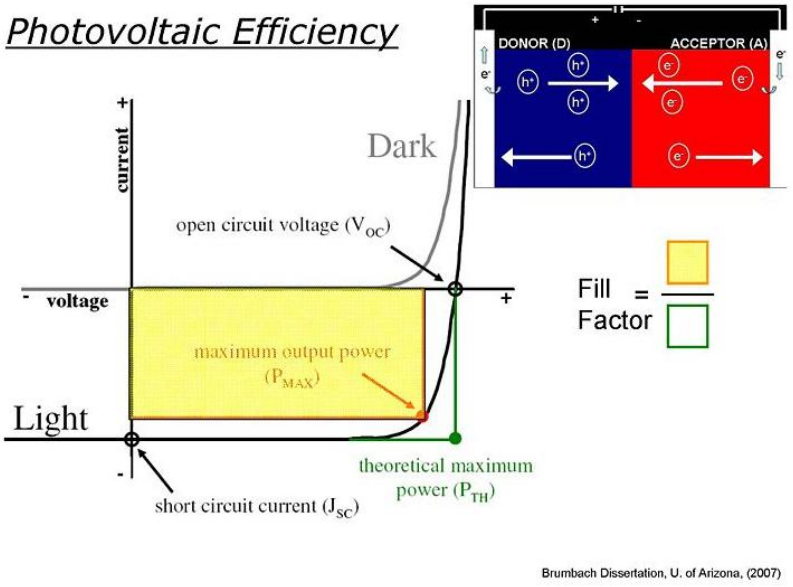

Figure 4.7 I-V curve with the schematic representation and the equation of Fill Factor, FF.

As FF is a measure of the "squareness" of the IV curve, a solar cell with a higher voltage has a larger possible FF since the "rounded" portion of the IV curve takes up less area. The maximum theoretical FF from a solar cell can be determined by differentiating the power from a solar cell with respect to voltage and finding where this is equal to zero. Hence:

$$\frac{\mathrm{d(IV)}}{\mathrm{dV}} = 0$$

giving:

$$V_{MP} = V_{OC} - \frac{nkT}{q}\ln\left(\frac{V_{mp}}{nkT/q} + 1\right) \qquad (1.7)$$

However, the above technique does not yield a simple or closed form equation. The equation above only relates V_{oc} to V_{mp}, and extra equations are needed to find I_{mp} and FF. A more commonly used expression for the FF can be determined empirically as:

$$\mathrm{FF} = \frac{\upsilon_{OC} - \ln(\upsilon_{OC} + 0.72)}{\upsilon_{OC} + 1} \qquad (1.8)$$

where υ_{oc} is defined as a "normalized V_{oc}":

$$\upsilon_{OC} = \frac{q}{nkT} V_{OC} \qquad (1.9)$$

A larger fill factor is desirable, and corresponds to an I-V sweep that is more square-like. Typical fill factors range from 0.5 to 0.82 [40]. Fill factor is also often represented as a percentage.

The above equations show that a higher voltage will have a higher possible FF. However, large variations in open-circuit voltage within a given material system are relatively uncommon. A key limitation in the equations described above is that they represent a maximum possible FF, although in practice the FF will be lower due to the presence of parasitic resistive losses[43]. Therefore, the FF is most commonly determined from measurement of the IV curve and is defined as the maximum power divided by the product of J_{sc}*V_{oc}, i.e.:

$$FF = \frac{P_{max}}{P_T} = \frac{J_{MP} V_{MP}}{V_{OC} J_{SC}} \qquad (1.10)$$

where P_{max} is the maximum power,

P_T is the theoretical power that would be output at both the open circuit voltage and short circuit current together,

J_{MP} is the current density for maximum power,

V_{MP} is the voltage for maximum power,

V_{OC} is the open circuit voltage and

J_{SC} is the short circuit current density.

4.4.5. Power conversion efficiency, PCE:

The efficiency is one of the three key factors for an efficient OSC device. It is the most commonly used parameter to compare the performance of one solar cell to another. Efficiency is defined as the ratio of energy output from the solar cell to input energy from the sun. In addition to reflecting the performance of the solar cell

itself, the efficiency depends on the spectrum and intensity of the incident sunlight and the temperature of the solar cell. Therefore, conditions under which efficiency is measured must be carefully controlled in order to compare the performance of one device to another. Terrestrial solar cells are measured under AM1.5 conditions and at a temperature of 25°C.

Efficiency is the ratio of the electrical power output P_{out}, compared to the solar power input, P_{in}, into the PV cell. P_{out} can be taken to be P_{MAX} since the solar cell can be operated up to its maximum power output to get the maximum efficiency.

$$\eta = \frac{P_{out}}{P_{in}} = \frac{P_{max}}{P_{in}} \quad (1.11)$$

The efficiency of a solar cell is determined as the fraction of incident power which is converted to electricity and is defined as:

$$P_{MAX} = V_{OC}\, I_{SC}\, FF \quad (1.12)$$

$$PCE = \frac{V_{OC} * J_{SC} * FF}{P_{INC}} * 100\% \quad (1.13)$$

Where, P_{INC} is the incident power density (sun power) ehich is equal to P_{INC}=100 mW/cm^2.

4.4.6. Hole mobility, μ:

Carrier mobility in a semiconductor is one of the most important parameters for the operation of electronic devices, OPVs included. The mobility measures the ability of free carriers (electrons or holes) to move in the material as it is subjected to an external electric field. Hole mobility is essentially the ability of a hole to move through a metal or semiconductor when electrical charge is applied.

The carrier mobility in a material is limited by various scattering mechanisms whose effect is to deviate the carrier trajectory or to absorb the energy gained by the carriers following the electric field acceleration. The electron mobility and hole mobility have a similar doping dependence: For low doping concentrations, the mobility is almost constant and is primarily limited by phonon scattering. At higher doping concentrations, the mobility decreases due to ionized impurity scattering with the ionized doping atoms[44].

The hole mobility of each fabricated device can be calculated using the equation below:

$$J_{SC} = \frac{9}{8} \frac{\mu \varepsilon_0 \varepsilon_r}{L^3} (V - V_{bi})^2 \Leftrightarrow$$

$$\mu = \frac{8}{9} \frac{J_{SC} L^3}{\varepsilon_0 \varepsilon_r (V - V_{bi})^2} \quad (1.14)$$

where μ is the hole mobility value, ε_0 is vacuum permittivity with a value of $\varepsilon_0 = 8.854 \times 10^{-12}$ F/m, ε_r is the relative permittivity, which for OPVs has a value of $\varepsilon_r = 3$ and L is the thickness of the PEDOT:PSS layer, with a value of 100nm. V is the measured electric potential and V_{bi} is the built in potential, which for PEDOT:PSS has a value of $V_{bi} = 0.3$V.

The built-in potential (or barrier potential) in a semiconductor equals the potential across the depletion region in thermal equilibrium. Since thermal equilibrium implies that the fermi energy is constant throughout the p-n diode, the internal potential must equal the difference between the fermi energies of each region. It also equals the sum of the bulk potentials of each region, since the bulk potential quantifies the distance between the fermi energy and the intrinsic energy. Therefore the expression for the built in potential of a semi-conductor is as follows:

$$V_{bi} = V_t \ln \frac{N_D N_A}{n_i^2} = \ln V_t \frac{N_D}{n_i} + \ln V_t \frac{N_A}{n_i} \qquad (1.15)$$

where N_A is the acceptor density of the p-type semiconductor and N_D is the donor density of the n-type semiconductor. The electron density in the n-type region is approximately equal to the donor density and the hole density in the p-type region is approximately equal to the acceptor density.

Chapter 5: Experimental Procedure

In the experiments carried out during this Diploma Thesis, the treatment of PEDOT:PSS (the HTL in conventional BHJ structure) with PFI and DMSO was examined. Firstly, the optimal PEDOT:PSS to PFI ratio was investigated. Once this was determined, the effects of DMSO were examined.

In this chapter, the steps followed in the fabrication of BHJ organic photovoltaic cells (conventional structure) will be presented and analyzed. There are five main steps in the fabrication process:

1. Four-step cleaning process of substrates.
2. Deposition and treatment of the PEDOT:PSS (HTL).
3. Deposition of PTB_7-$PC_{60}BM$ (Active Layer blend).
4. Deposition of Calcium Interlayer (ETL) and the Aluminum Cathode.

5.1. Conditions of the experiment:

The first two steps of the experimental procedure took place outside the inert atmosphere which the glove box provides. However, great care was taken so that dust particles didn't land on the substrates (i.e. the devices were always kept in a covered Petri dish and a pressure air gun was used to remove dust particles before the deposition of layers began). Any dust landing on the OPV device leads to "dead spots" on its surface. This means that the device's working operation stops where the dust has landed on the surface, which is typically a very small fraction of the area. So, OPVs are generally tolerant of dust due to its insulating nature and therefore it is possible for fabrication to take place outside of a glove-box as long as extra care is taken. A problem that can occur due to dust particles is the change in wetting properties on the surface area where dust has landed. This occurrence leads to pinholes on the substrates surface and therefore a decrease in device efficiency. This has to be taken into account during the deposition of PEDOT:PSS-PFI via spin coating. This stage cannot be performed inside the glove box because of the humidity produced after the removal of water-solvent from the PEDOT:PSS:PFI mixture.

Figure 5.1 The glove boxes utilised throughout the experimental procedure. Glove Box No1 (right) contains the UV-O3 cleaner and the spin coater used for the deposition of the active layer. Glove Box No2 (left) contains the Vacuum Thermal Evaporator used for the deposition of the Ca Interlayer and Ag cathode.

It should be noted that PEDOT:PSS is a hydroscopic mixture which means it easily absorbs moisture from the atmosphere. This may possibly lead to a phase separation of PEDOT from PSS and as a result a rapid degradation of the devices performance. The absorption of moisture also increases the existing oxidative character of PEDOT:PSS, which affects to the next layer, the active layer. This is why after the deposition of PEDOT:PSS:PFI and the thermal removal of the water solvent, the devices are transferred inside the glove box where they are protected from the water and oxygen molecules of the air outside.

The active layer can also be degraded by oxygen and water, especially in the presence of light. This is the reason why the last three steps of the experimental process take place inside glove box with the box light off. On one hand, the inert nitrogen atmosphere of the glove box protects the devices from moisture and oxygen. On the other hand, processing under very low light minimizes the exposure time of the devices, therefore preserving their stability. The Calcium interlayer, which acts as the ETL, is especially reactive in atmospheric conditions.

5.2. Handling of the substrates:

The ITO-glass substrates must be thoroughly cleaned, as will be described below, and handled with care using tweezers (Figure 5.2). There are specific areas on the substrates from which they can be held with tweezers. The active areas must avoid being touched, as this will scratch the thin-layer materials applied causing shorting of the anode and cathode (Figure 5.3).

Figure 5.2 The tweezers used for the handling of the substrates.

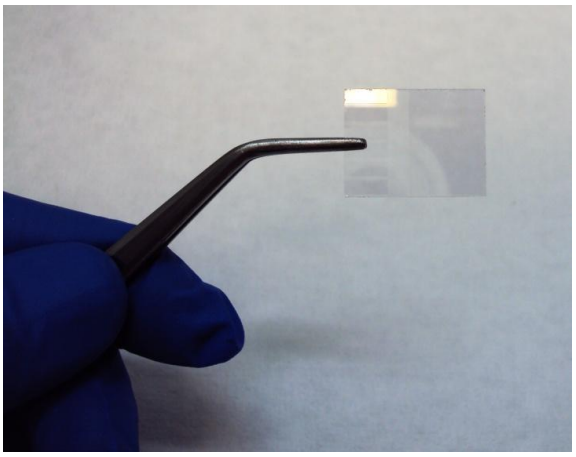

Figure 3.3 The correct area to position the tweezers in order to avoid touching the active area.

Figure 5.4 Multimeter used to ensure that the ITO-glass substrates are facing upwards.

It is also vital that the substrates remain right side up throughout the experiment. In order to recognize the right side, which is the side with the ITO layer, a multimeter is used (Figure 5.4), since ITO is transparent and therefore almost invisible to the naked eye. If the active area comes into contact with any other surface, then the substrate is considered chemically unclean leading to device defects due to pollution (e.g. from dust particles). Any

substrates which have been dropped and have landed active side down are considered chemically unclean and are discarded.

5.3. Four step cleaning method:

As mentioned previously, the glass substrates that were purchased already have the ITO anode applied. Before the deposition of the rest of the material layers can begin, the ITO-glass substrates must be thoroughly cleaned. This is the cleaning method used:

- *First step:* The substrates are first inserted into a holder (Figure 5.5) with the ITO-coated side facing in the same direction. The holder is then submerged into soap water (deionised water to be exact) inside a 1000ml beaker (Figures 5.5, 5.6). The beaker is then put into an ultrasonic bath at room temperature for 10 minutes (Figure 5.7).

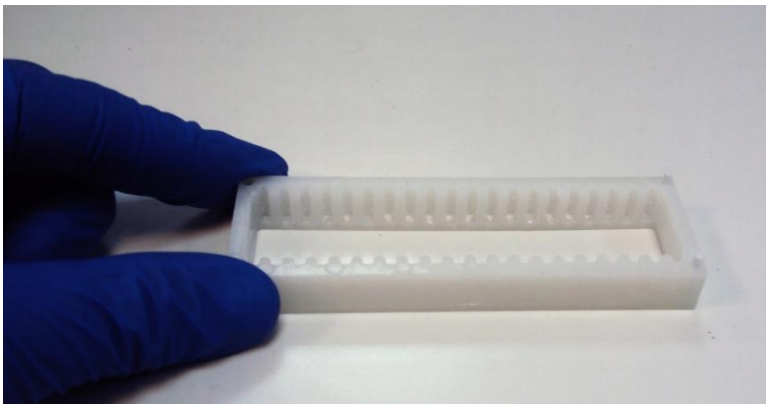

Figure 5.5 Substrate holder which holds 20 substrates.

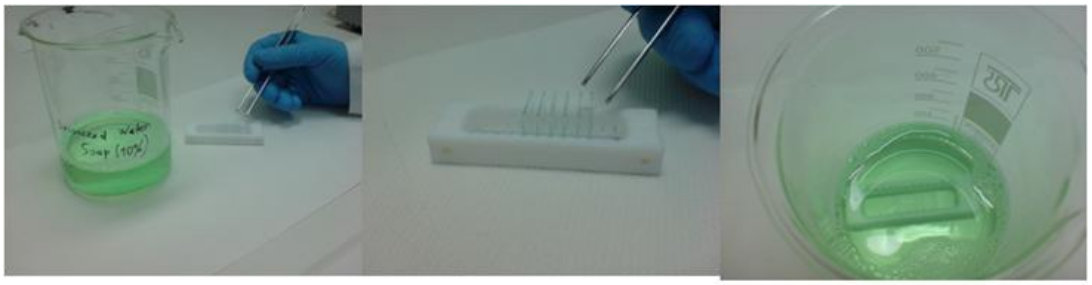

Figure 5.6 Insertion of the substrates into the holder and submersion in soap water.

The substrates are then thoroughly rinsed with deionised water as to remove all traces of soap.

- *Second step:* The holder is submerged in acetone in a different 1000ml beaker. The beaker is again put in an ultrasonic bath at room temperature for 10 minutes
- *Third step:* The holder is taken out of the acetone and submerged in isopropanol (2-propanol, IPA) in a 1000ml beaker which is then put in a last ultrasonic bath again at room temperature for 10 minutes. The substrates are then transferred from the holder to a Petri dish with the ITO side facing up. The Petri dish is placed in an oven at 120°C for 15 minutes in order for the substrates to dry (Figure 5.8).

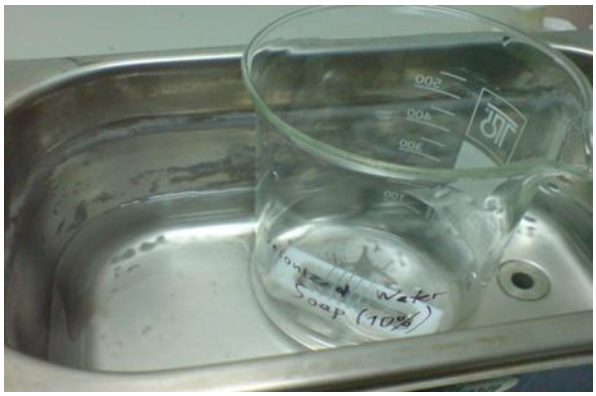

Figure 5.7 Ultrasonic bath.

Figure 5.8 Placement of devices in the oven (120°C for 15 minutes) after cleaning.

- *Fourth step:*

The fourth and last step of the cleaning process is the placement of the substrates inside a vacuum UV-Ozone cleaner chamber for 15 minutes at about 1mW/cm^2. This process not only removes any organic contamination, but it also increases the surfaces' hydrophilicity, which increases its affinity to the water solved PEDOT:PSS layer which is to be applied next. The UV-O_3 cleaner (shown in Figure 5.9) is located inside the laboratory's glove box.

Figure 5.9 Manual MBRAUN MB-UV-O_3-Cleaner

After the UV-O_3 treatment is over, the deposition of the HTL must take place as soon as possible, as the hydrophilic properties acquired wear off with time.

Figure 5.10 Settings screen of MBRAUN UV-O3 cleaner

Figure 5.11 Air flow settings of MBRAUN UV-O3 Cleaner.

5.4. Deposition of Hole transport layer (HTL)-Treatment of HTL:

As mentioned earlier, PEDOT:PSS treated with PFI was used as the Hole Transport-Electron Blocking Layer. This material is applied using the spin coating method, which is a useful technique for deposition of thin uniform films on planar substrates.

5.4.1. Preparation of the PEDOT:PSS solution treated with PFI:

The PEDOT:PSS solution is kept in a refrigerator for preservation, so before use, it must be allowed to reach room temperature. Then, PEDOT:PSS is filtered into a 4ml clear glass vial using a syringe and a 0.45 μm PVDF filter to remove any impurities. The syringe used is rubber free, as many rubbers are attacked by the acidic nature of the PEDOT:PSS. The desired amount of PFI is added to the PEDOT mixture using a Gilson pipette.

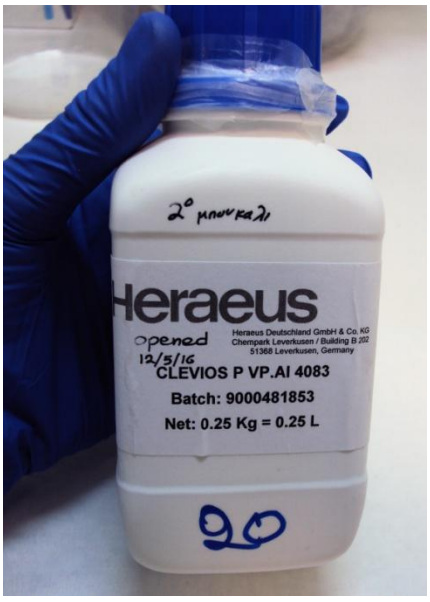

Figure 5.12 PEDOT:PSS purchased from Clevios.

Figure 5.13 Tetrafluoroethylene-perfluoro-3,6-dioxa-4-methyl-7-octenesulfonic acid copolymer (PFI or Nafion™)

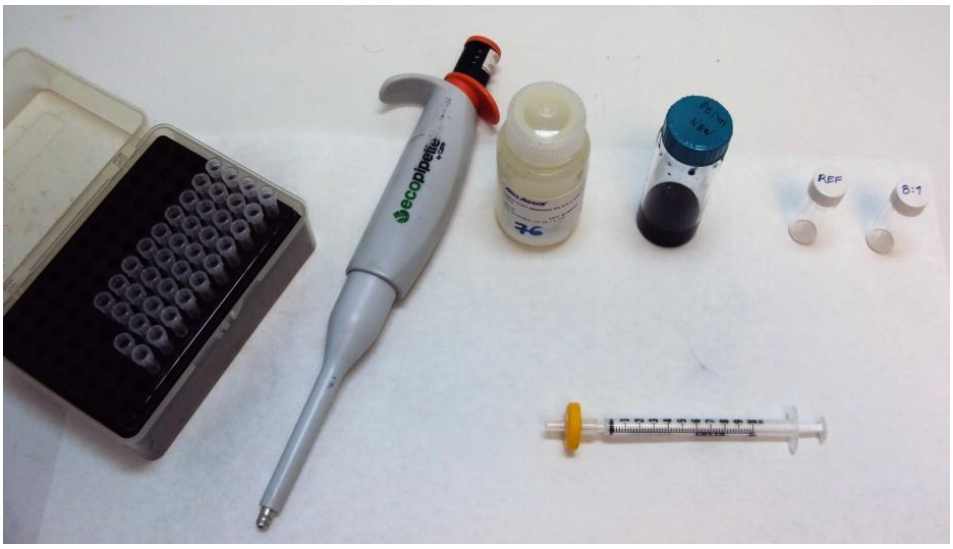

Figure 5.14 Utensils and materials used in the preparation of the PEDOT:PSS-PFI solutions.

5.4.2. <u>Deposition of PEDOT:PSS:PFI via static spin coating method:</u>

PEDOT:PSS:PFI is applied using the static spin coating method. Firstly, the device is set to spin the substrate at 5000rpm for 60 seconds. (Figure ...). The substrate is then positioned ITO-side up on the rotation mechanism. It is held in place via vacuum suction. 300µL of the solution is placed on the substrate via Gilson Pipette. The substrate is rotated at an adjustable angular velocity resulting in the spreading of the liquid due to centripetal force.

Figure 5.15 Spin coater used for the deposition of the HTL.

Figure 5.16 Settings screen of spin coater. Substrates were set to spin for 60 seconds at 5000rpm.

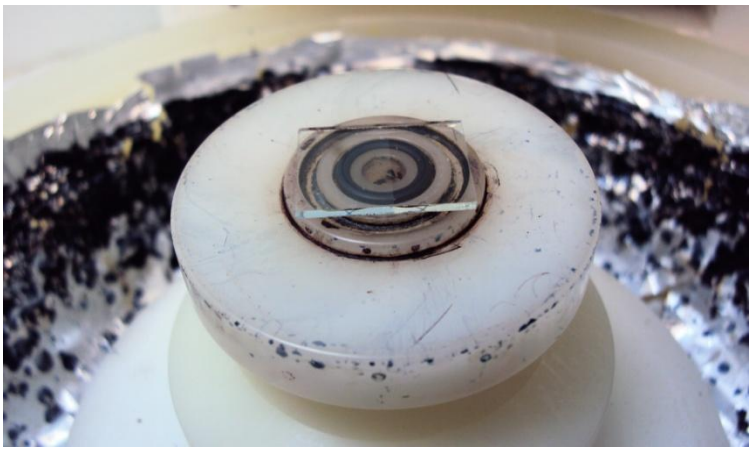

Figure 5.17 Proper positioning of the glass substrate on the rotation mechanism.

The rotation continues for an adjustable time. The time and the speed of rotation determine the amount of solution that will remain on the substrate and hence the layer thickness. The theoretical layer thickness can be calculated using Formula 5.1 , where t is the layer thickness, η is the viscosity of material in connection with the concentration (c) and angular rotational velocity (ω). However, as field emission experiments have shown, the layer thickness for PEDOT:PSS is typically about 30nm.

$$t = \frac{\eta(c)}{\sqrt{\omega}} \qquad (5.1)$$

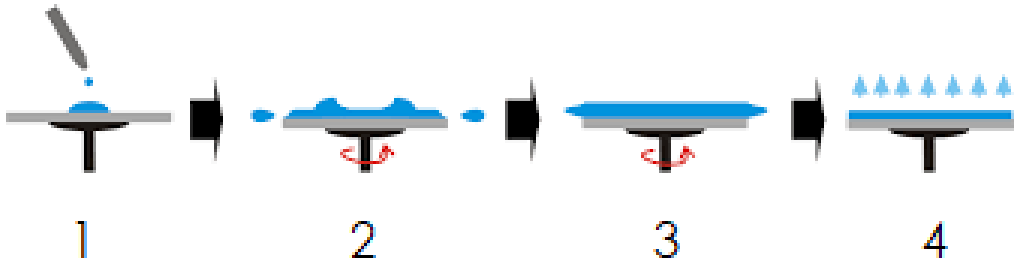

Figure 5.18 The spin coating method. 1) The solution is applied. 2) As the substrate is rotated, the solution spreads. 3) A thin layer is acquired. 4) Humidity is thermally removed.

When the spin coating procedure has finished, a strip of PEDOT:PSS:PFI from the top and bottom section of the substrate is wiped away with a cotton bud soaked in deionised water (Figure 5.19). This strip is removed in order to ensure that the electrode comes into contact with the ITO layer without the HTL blocking it.

After this wiping process, the substrates are placed in an oven at 120ºC for 15 minutes in order to remove the humidity.

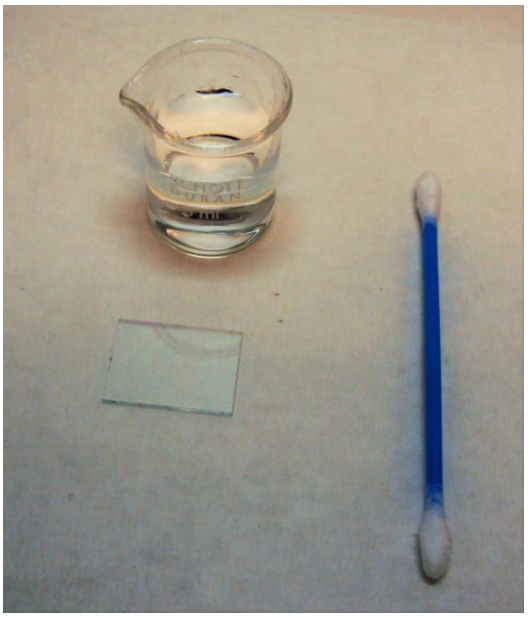

Figure 4.19 A regular cotton bud soaked in deionised water is used to wipe PEDOT:PSS and PEDOT:PSS-PFI from the top and bottom area of the ITO-glass substrate.

5.4.3. Treatment of PEDOT:PSS layer with DMSO bath:

After the substrates are removed from the oven, one of them is treated with a Dimethyl-sulfoxide (DMSO) bath for 30 minutes (Figure 5.21). After this, the substrate is placed on a hotplate for 10 minutes at 120°C to remove the excess DMSO. A second wiping procedure with a cotton swab takes place to make sure that none of the PEDOT:PSS-PFI was washed toward the electrodes by the DMSO bath.

Figure 5.20 Equipment used for treatment of substrates with DMSO.

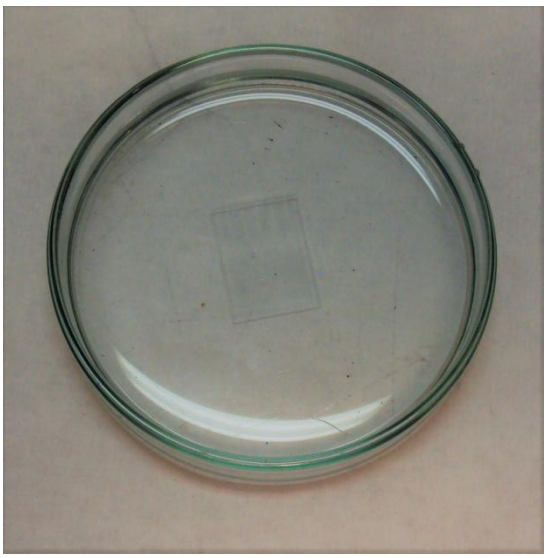

Figure 5.21 Substrate in DMSO bath.

All three substrates are then transferred into the glove box, where they are placed on a hotplate at 120°C for 30 minutes for thermal annealing. After being left to reach room temperature (about 10 minutes) they are then ready for the deposition of the next layer. The rest of the experimental procedure takes place inside the glove box. It is important that after the deposition of the PEDOT:PSS, exposure to air must be minimal as the humidity in the atmosphere can have a negative effect on this material and therefore the devices' performance.

5.5. Deposition of the Active Layer:

The active layer used was the polymer-fullerene derivative blend PTB_7-$PC_{60}BM$..

5.5.1. Preparation of the Active Layer Blend:

The following procedure is for the preparation of 1ml of polymer-fullerene blend.

Firstly, 10μg of PTB_7 are weighed and added to 970μL of anhydrous Chlorobenzene (CB) in a 2ml clear vial. The solution is stirred for 1 hour at 75°C. When the hour is up, 15μg of $PC_{60}BM$ are added to the solution which is stirred over night at 75°C. While the solution is left to be stirred, it must be kept under dark conditions in order to minimize light exposure of the material.

After being left overnight, *3,3'-dioctadecyloxacarbocyanine (DIO*), purchased from Sigma-Aldrich, is then added to the blend which is again left to be stirred at 70°C under dark conditions for 1 hour. The materials and appliances used in the preparation of this blend are shown in Figures 5.23-5.25.

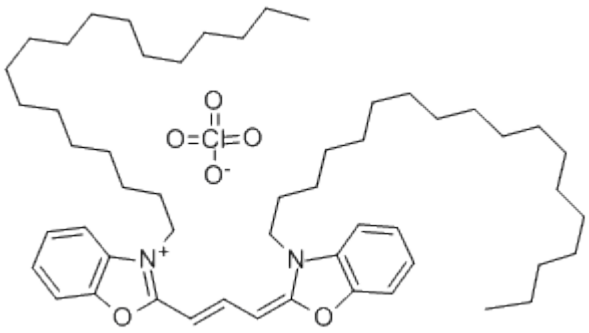

Figure 5.22 Chemical structure of DIO

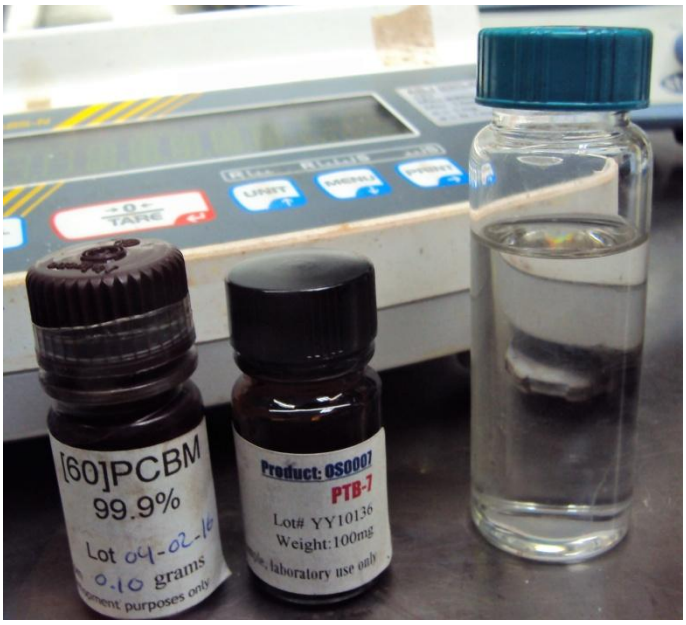

Figure 5.23 PTB_7, $PC_{60}BM$ and anhydrous Chlorobenzene

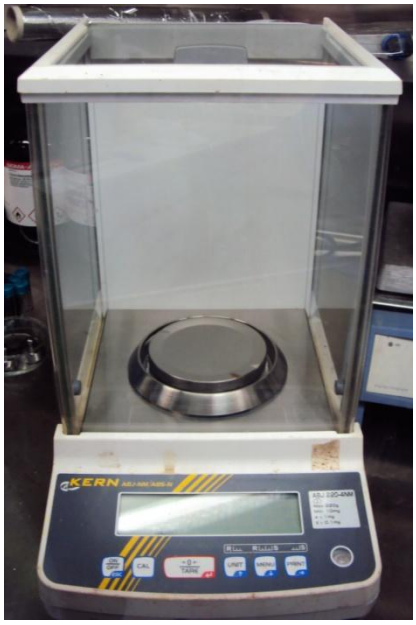

Figure 5.24 Analytical balance used for weighing PTB_7 and $PC_{60}M$ powder.

Figure 5.25 The PTB_7-$PC_{60}BM$ blend is kept under dark conditions stirring on a hotplate at 70°C overnight.

5.5.2. <u>Deposition of PTB_7-$PC_{60}BM$ via dynamic spin coating method:</u>

The spin coating method for this layer is a little bit different than that used for the HTL. Firstly, as mentioned earlier, it takes place inside the

glove box. Secondly, unlike with PEDOT:PSS, the active layer is applied using the dynamic spin coating method. This method is different than that of the static spin coating procedure, in that the substrate is first set into rotation and then the solution is applied all while the rotation is in motion.

The spin coater used was the Ossila Spin Coater (Figure 5.26). The substrates were set to spin at 2500rpm for 30 seconds. Field emission measurements have shown that these settings typically result in a layer thickness of about 80-100nm.

Figure 5.26 Spin coater inside Glove Box No1 used for the deposition of the PTB_7-$PC_{60}BM$ active layer blend.

For the application of the active layer blend the substrate is placed in the slot and 50μl of the solution are acquired with a Gilson pipette. The substrate is then set into rotation and the blend is applied. After the active layer has been deposited, the substrates are placed in an active vacuum for 20 minutes in order for the solute to be removed. The top and bottom layer of each substrate is then wiped with a cotton swab soaked in chloroform (CF). The PTB_7-$PC_{60}BM$ is removed in these areas so the cathode comes into contact with the ITO layer. It should be noted that during this procedure the gloves of the glove boxμare covered by a pair of disposable gloves, as they can be damaged by organic solvents such as CF.

When this procedure is done, the substrates are ready to undergo the deposition of the Calcium interlayer and then the Silver cathode.

5.6. Deposition of the Ca interlayer-ETL and the Ag cathode:

The Calcium and Silver layers are deposited via vacuum thermal evaporation (VTE). The thermal vacuum evaporator is located inside a glove box ensuring that atmosphere sensitive materials remain stable. The thermal vacuum evaporator is shown in Figure 5.27

Figure 5.27 Thermal vacuum evaporator located inside a glove box.

In this process, Ca and Ag pellets, are placed (one material at a time) in a cavity enclosed within a vacuum chamber. The substrate that is to become the coating is placed on a special base, which is known as a "boat", over the cavity. The cavity is supplied with a current and, due to its Ohmic resistance, it is heated. The metal pellets melt and evaporate. The vaporized molecules of the material overlay on the substrate and form the coating. The coating thickness depends on the distance of the substrate from the cavity (source evaporation) and the time of supply with electricity. The overlay can be made on specific parts of the substrate with the use of shadow masks (shown in Figure 5.28), This mask leaves only the area we wish to coat exposed.

Figure 5.28 Shadow mask in which the substrates are placed in order to undergo metal deposition via VTE method.

Firstly, 5nm of Ca are deposited onto the substrates. Then 100nm of Ag are evaporated to form the cathode.

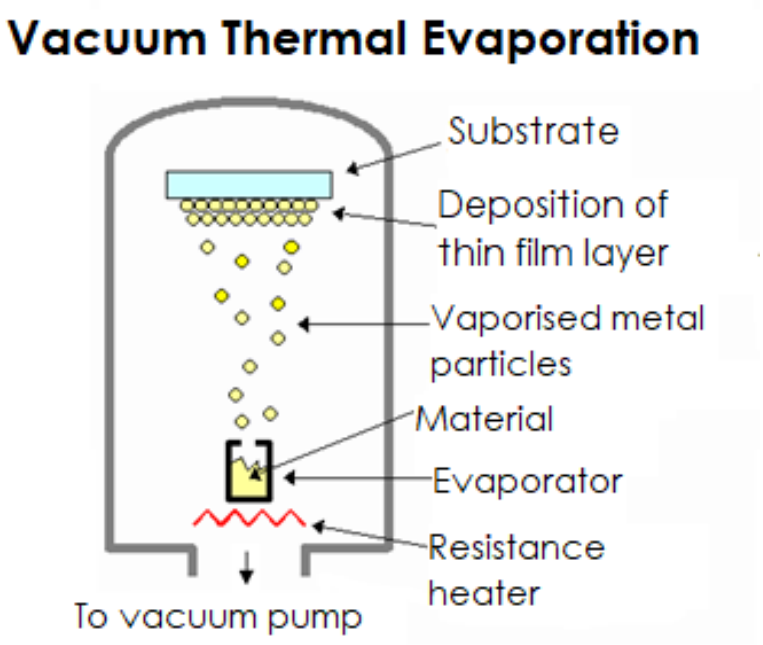

Figure 5.29 Schematic representation of deposition via Vacuum Thermal Evaporation method.

5.7. Device characterisation:

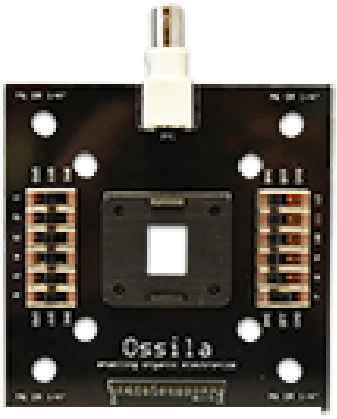

Figure 5.30 The test board used for making electrical connections to the photovoltaic devices.

The performance of the devices can be described by measuring their current versus voltage (*I–V*) under conditions of light using a solar light simulator. The most common performance indicator is the photovoltaic efficiency (PVE) under standard reporting conditions (SRC) (temperature, spectral irradiance and total irradiance) and it is equal to the maximum electrical power divided by the total irradiance (1000 W/m^2). A computer controlled voltage and current sources provide the voltage difference and the current across the device. A lamp, which simulates the solar spectrum, illuminates the OPV device under AM 1.5 conditions throughout the characterization process. First, the lamp is

turned on and the power is set in order to act as sun simulator (100mW/cm^2), the device is placed into the characterization set-up and the necessary wiring follows.). Initially, we bring together two metal probes of Ossila test board, shown in Figure 5.30**.** The whole layout is covered with a black box in order to start the measurement process under dark conditions. The *Easy EXPERT software* is launched, solar cell mode is selected, the range and voltage are set and finally the corresponding current-voltage curve is obtained in the dark. The algorithm of the program calculates important values for solar cells like current density (J) and short circuit current density (J_{sc}), open circuit voltage (V_{oc}), maximum efficiency ($P_{max)}$, fill factor (FF), cell efficiency (PCE%).

Chapter 6: Results and discussion

6.1. Examining the effects of two step treatment of PEDOT:PSS on the photovoltaic characteristics:

As mentioned in Chapter 5, the first device characterisation that was performed was the measurement of the short circuit current density (J_{sc}), open circuit voltage (V_{oc}), fill factor (FF) and cell efficiency (PCE%) using a solar simulator. These photovoltaic characteristics can be seen in Table 6.1. A current density-voltage (J-V) graph was then constructed (Figure 6.1). The next characteristic to be calculated was hole mobility (μ) (see Table 6.1 and Figure 6.2) , using equation 1.14 in Chapter 4. The morphology of each PEDOT:PSS film was then recorded using Atomic Force Microscopy (AFM) topography.

Table 6.1 Photovoltaic characteristics and hole mobilities for the reference device, the PFI-treated and the PFI-DMSO treated devices.

	Jsc (mA/cm^2)	Voc (V)	FF (%)	PCE (%)	μ_h ($cm^2V^{-1}s^{-1}$)
Ref	16.4	0.76	47.0	5.91	1.25×10^{-4}
PEDOT:PSS/PFI (8:1)	**17.0**	0.76	**47.4**	**6.13**	**1.82×10^{-4}**
PEDOT:PSS/PFI (8:1) + DMSO	**17.8**	0.76	**49.3**	**6.41**	**3.4×10^{-4}**

It is clear that the PCE was increased by the two step treatment method. More specifically, the PCE was increased from 5.91% to 6.13% by the addition of PFI to the PEDOT:PSS layer, showing an improvement of 3.72% compared to the reference device. This effect was further enhanced with the DSMO treatment in which case the PCE increased from 5.91% to 6.41%, thus displaying an 8.46% improvement compared to the reference device.

The open circuit voltage (V_{OC}) of all of the devices was kept as a constant at 0.76V.

Knowing the electrical J-V characteristics of a solar cell is critical in determining the device's output performance and solar efficiency. Solar Cell I-V Characteristics Curves are basically a graphical representation of the operation of a solar cell or module summarising the relationship between the current and voltage at the existing conditions of irradiance and temperature. I-V curves provide the information required to configure a solar system so that it can operate as close to its optimal peak power point (MPP) as possible. The J-V curve for all three cells can be seen in Figure 6.1. The slope for each curve increases as we move from the reference to the PFI/DMSO curve. This indicates an increase in the value of the fill factor. The Jsc is increased by 0.6 mA/cm^2 and 1.4 mA/cm^2 for the PFI and PFI/DMSO treated HTLs respectively in comparison to the reference solar cell.

The fill factor was increased from 47% to 47.4% and 49.3% for the PFI and the PFI/DMSO treated HTLs respectively. This increase of the FF can be attributed to the increase in J_{SC}, since the value of V_{OC} remains constant.

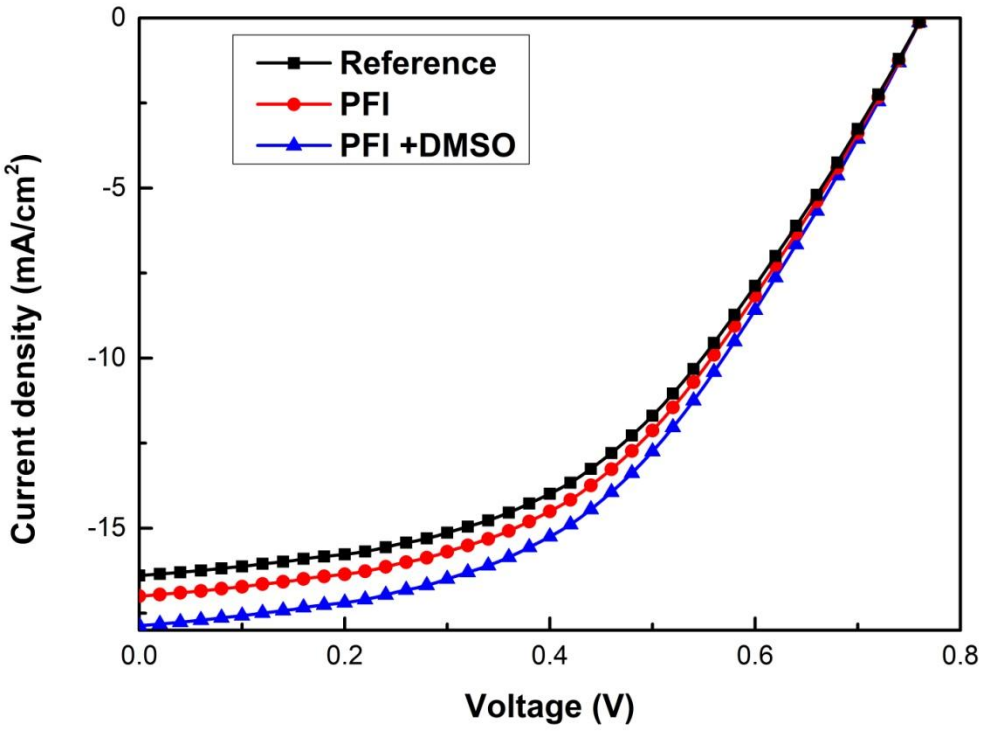

Figure 6.1 J-V characteristics under "one sun" illumination (100 mW/cm^2) for the optimized devices including the reference device (PEDOT:PSS), the PFI-treated device (PEDOT:PSS/PFI) and the PFI-DMSO treated device (PEDOT:PSS/PFI – DMSO).

In order to measure and compare the hole mobility in pristine PEDOT:PSS and the treated PEDOT:PSS films, hole-only devices were fabricated comprised of only the ITO anode, the PEDOT:PSS HTL, the PTB_7-$PC_{60}BM$ active layer, a Molybdenum(VI) oxide (MoO_3) HTL and the Ag cathode (in that order). These hole-only devices were then measured using a solar simulator under dark conditions. The hole mobility (μ_h) values are featured in Table 6.1 and the respective J-V graph is shown in Figure 6.2. Results showed that the μ_h increased from 1.25 x 10^{-4} $cm^2V^{-1}s^{-1}$ to 1.82 x 10^{-4} $cm^2V^{-1}s^{-1}$ for PFI treated PEDOT:PSS film and to 3.4 x 10^{-4} for the PEDOT:PSS film that underwent an additional DMSO treatment. This observed increase in hole mobility means that the hole, which originates from the PTB_7 of the active layer blend, could be easily extracted for device based on PEDOT:PSS/PFI and even easier from the device based on PEDOT:PSS/PFI-DMSO. The enhanced μ_h corresponds to the increase of the fill factor (FF).

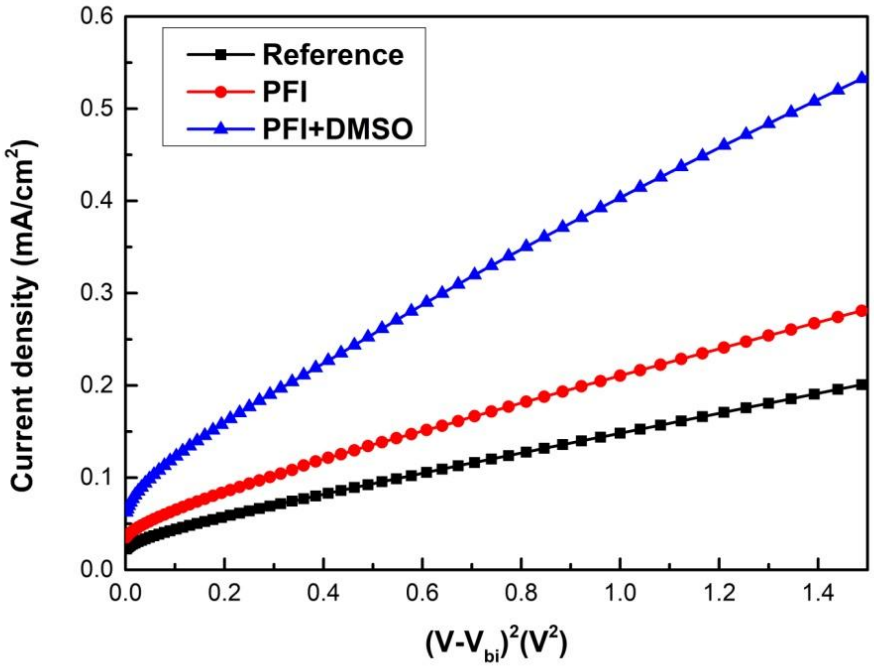

Figure 6.2 The J-V graph plotted for the investigation of the hole mobilities of the reference device, the PFI-treated and the PFI/DMSO-treated devices.

6.2. Examining the effects of two step treatment of PEDOT:PSS on the morphology of the HTL:

In previous studies it has been shown that in a solution, PEDOT:PSS forms micelles around a PEDOT crystalline core, which has been shown by scattering techniques to grow when PEDOT:PSS is subject to solvent

treatments[27]. Once spin-coated, AFM images have revealed bright and dark areas, which are commonly associated with PEDOT and PSS rich regions[27][45][46]. In the case of the mixed materials, PSS and the fluorination agents compete to stabilize the PEDOT polymeric chains. The morphology of the images is noticeably influenced by the presence of the fluorination agent leading to larger bright domains. This feature is more visible with the polymeric than with the surfactant fluorination.

In the AFM morphology characterisation performed in this experiment, the roughness of the HTL was shown to be increased with the PFI treatment in comparison to the reference device. More specifically the roughness for the PFI treated HTL had a value of R_{MS}=1.204 nm, whereas the reference device had a roughness value of R_{MS}=0.882 nm, therefore showing an increase of 0.332 nm. The increase in roughness was further enhanced with the additional DMSO bath treatment, where the respective device showed an HTL roughness of R_{MS}=3.220 nm, therefore showing an increase of 2.338 nm.

The surface AFM images for each PEDOT:PSS film can be seen in Figure 6.3. The increasing surface roughness shows the improved crystallization of PEDOT:PSS. A higher roughness of the HTL not only ensures a larger interface between the HTL and the active layer, but also minimizes the occurrence of traps or electron-hole re-combinations.

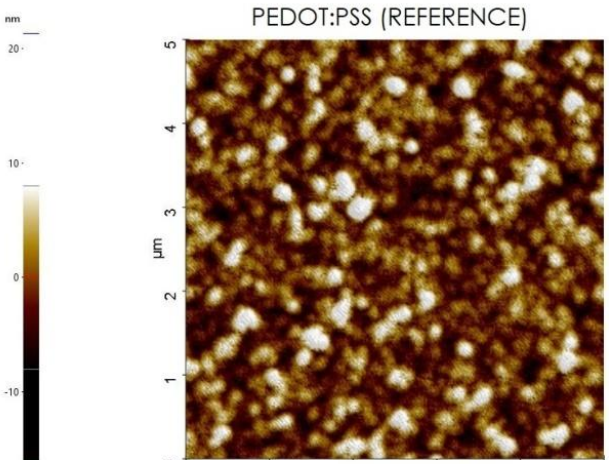

Figure 5.3 Morphology of the reference HTL shown via AFM imaging.

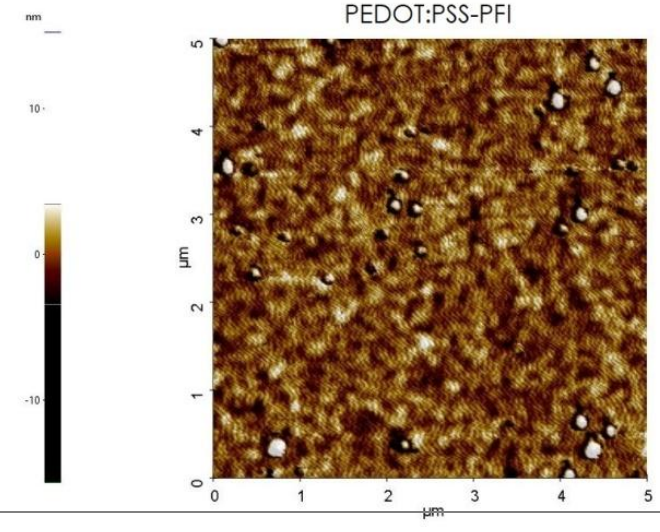

Figure 6.4 Morphology of the PFI-treated HTL shown via AFM imaging.

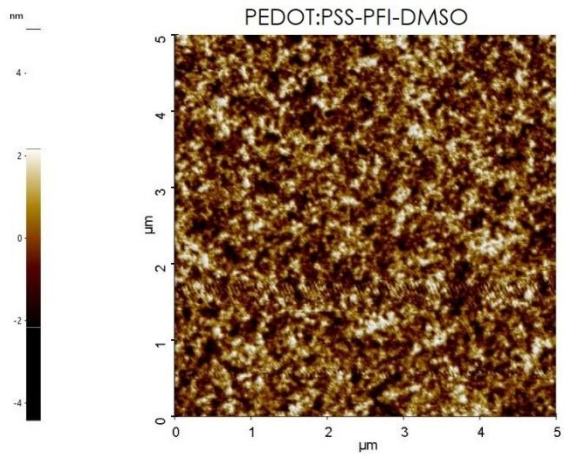

Figure 6.5 Morphology of the PFI/DMSO-treated HTL as shown through AFM imaging.

Conclusions:

The present Diploma Thesis successfully captures the fabrication processes followed in the constructions of an organic photovoltaic device. It investigates the effects of fluorination and organic solvent treatment on the PEDOT:PSS Hole Transport/Electron Blocking Layer in regards to its performance as such. As analyzed in Chapter 6, even though this two-step treatment method increases the photovoltaic characteristics of the OPV device, enhances the hole mobility in the HTL and has positive effects on the morphology of this layer, these aspects of the OPV device were improved slightly and the results seem to stand off from a more desirable solar cell performance.

The enhanced photovoltaic characteristics and the overall performance of the treated solar cells can be attributed to the increased hole mobility due to the addition of PFI polymer and the improved morphology thanks to the treatment with DMSO solvent.

The effects of fluorination and organic solvent treatment on PEDOT:PSS have been investigated in past experiments. This is a treatment method that undoubtedly produces positive results is a useful approach towards extending the spectral range of enhanced light harvesting in OPVs. However, in order to enhance this improved performance, perhaps this treatment of the PEDOT:PSS HTL can be paired with a more complementary active layer blend. Furthermore, there are other organic solvents that can be utilized instead of DMSO, as shown in past literature, as well as other fluorination mediums besides PFI.

Bibliography:

[1] "Introduction to Renewable Energy | EnvironmentalScience.org." [Online]. Available: http://www.environmentalscience.org/renewable-energy. [Accessed: 10-Oct-2017].

[2] D. R. Myers, K. Emery, and C. Gueymard, "Revising and Validating Spectral Irradiance Reference Standards for Photovoltaic Performance: Preprint," 2002.

[3] "Energy Education." [Online]. Available: http://energyeducation.ca/encyclopedia/Main_Page. [Accessed: 19-Oct-2017].

[4] "The Energy Conversion Process," *MRS Bull. @BULLET*, vol. 30, 2005.

[5] "3 Generations of Solar Cells: Solar Facts and Advice." [Online]. Available: http://www.solar-facts-and-advice.com/solar-cells.html. [Accessed: 19-Oct-2017].

[6] F. C. Krebs *et al.*, "Freely available OPV-The fast way to progress," *Energy Technol.*, vol. 1, no. 7, pp. 378–381, Jul. 2013.

[7] P. C. Choubey, A. Oudhia, and R. Dewangan, *Recent research in science and technology : an international refereed journal for all aspects of science research.*, vol. 4, no. 8. Recent Research in Science and Technology, 2009.

[8] M. Tawheed Kibria, A. Ahammed, and S. Mahmud Sony, "A Review: Comparative studies on different generation solar cells technology," 2014.

[9] P. C. Choubey, A. Oudhia, and R. Dewangan, "A review: Solar cell current scenario and future trends," *Recent Res. Sci. Technol.*, vol. 4, no. 8, pp. 99–101, 2012.

[10] M. A. Green, K. Emery, Y. Hishikawa, and W. Warta, "Solar cell efficiency tables (Version 34)," *Prog. Photovoltaics Res. Appl.*, vol. 17, no. 5, pp. 320–326, Aug. 2009.

[11] "Dye-sensitized solar cells," *J. Photochem. Photobiol. C Photochem. Rev.*, vol. 4, no. 2, pp. 145–153, Oct. 2003.

[12] M. Hosseinnezhad, "Cosensitization with Vat-Based Organic Dyes for Enhanced Spectral Response of Dye-Sensitized Solar Cells," *J. Electron. Mater.*, vol. 46, no. 4, pp. 2290–2295, Apr. 2017.

[13] Z. He *et al.*, "Single-junction polymer solar cells with high efficiency and photovoltage," *Nat. Photonics*, vol. 9, no. 3, pp. 174–179, Feb. 2015.

[14] B. O'Regan and M. Grätzel, "A low-cost, high-efficiency solar cell based on dye-sensitized colloidal TiO2 films," *Nature*, vol. 353, no. 6346, pp.

737–740, Oct. 1991.

[15] Y. Lin, Y. Li, and X. Zhan, "Small molecule semiconductors for high-efficiency organic photovoltaics," *Chem. Soc. Rev.*, vol. 41, no. 11, p. 4245, Jun. 2012.

[16] H. Spanggaard and F. C. Krebs, "A brief history of the development of organic and polymeric photovoltaics ARTICLE IN PRESS," *Sol. Energy Mater. Sol. Cells*, vol. 83, pp. 125–146, 2004.

[17] † Ivan G. Scheblykin, † Arkady Yartsev, † Tonu Pullerits, ‡ and Vidmantas Gulbinas, and † Villy Sundström*, "Excited State and Charge Photogeneration Dynamics in Conjugated Polymers," 2007.

[18] H. Kuzmany, J. Fink, M. Mehring, and S. Roth, *Electronic Properties of Fullerenes : Proceedings of the International Winterschool on Electronic Properties of Novel Materials, Kirchberg, Tirol, March 6-13, 1993*. Springer Berlin Heidelberg, 1993.

[19] G. Paterakis, "Photovoltaic structures and devices using polymer materials and graphene layers." .

[20] B. P. Rand and H. Richter, *Organic solar cells : fundamentals, devices, and upscaling*. .

[21] L. Zhao *et al.*, "The Effects of Improved Photoelectric Properties of PEDOT:PSS by Two-Step Treatments on the Performance of Polymer Solar Cells Based on PTB7-Th:PC $_{71}$ BM," *ACS Appl. Mater. Interfaces*, vol. 8, no. 1, pp. 547–552, Jan. 2016.

[22] S. H. Eom *et al.*, "Polymer solar cells based on inkjet-printed PEDOT:PSS layer," *Org. Electron.*, vol. 10, no. 3, pp. 536–542, May 2009.

[23] J. P. Thomas, L. Zhao, D. McGillivray, and K. T. Leung, "High-efficiency hybrid solar cells by nanostructural modification in PEDOT:PSS with co-solvent addition," *J. Mater. Chem. A*, vol. 2, no. 7, p. 2383, Jan. 2014.

[24] A. M. Nardes, M. Kemerink, M. M. de Kok, E. Vinken, K. Maturova, and R. A. J. Janssen, "Conductivity, work function, and environmental stability of PEDOT:PSS thin films treated with sorbitol," *Org. Electron.*, vol. 9, no. 5, pp. 727–734, 2008.

[25] B. Xu *et al.*, "Functional solid additive modified PEDOT:PSS as an anode buffer layer for enhanced photovoltaic performance and stability in polymer solar cells.," *Sci. Rep.*, vol. 7, p. 45079, 2017.

[26] H. Huang and J. Huang, *Organic and hybrid solar cells*. .

[27] C. T. Howells *et al.*, "Enhanced organic solar cells efficiency through electronic and electro-optic effects resulting from charge transfers in polymer hole transport blends," *J. Mater. Chem. A*, vol. 4, no. 11, pp. 4252–4263, Mar. 2016.

[28] S. Woo, H.-K. Lyu, Y. S. Han, and Y. Kim, "Effects of Hole-Collecting Buffer Layers and Electrodes on the Performance of Flexible Plastic Organic Photovoltaics," *Int. J. Photoenergy*, vol. 2013, pp. 1–8, Aug. 2013.

[29] J. Gasiorowski, R. Menon, K. Hingerl, M. Dachev, and N. S. Sariciftci, "Surface morphology, optical properties and conductivity changes of poly(3,4-ethylenedioxythiophene):poly(styrenesulfonate) by using additives.," *Thin Solid Films*, vol. 536, no. 100, pp. 211–215, Jun. 2013.

[30] A. M. Nardes *et al.*, "Microscopic Understanding of the Anisotropic Conductivity of PEDOT:PSS Thin Films," *Adv. Mater.*, vol. 19, no. 9, pp. 1196–1200, May 2007.

[31] I. Cruz-Cruz, M. Reyes-Reyes, M. A. Aguilar-Frutis, A. G. Rodriguez, and R. López-Sandoval, "Study of the effect of DMSO concentration on the thickness of the PSS insulating barrier in PEDOT:PSS thin films," *Synth. Met.*, vol. 160, no. 13–14, pp. 1501–1506, Jul. 2010.

[32] A. Dearden *et al.*, "Comparison of dimethyl sulfoxide treated highly conductive poly(3,4-ethylenedioxythiophene):poly(styrenesulfonate) electrodes for use in indium tin oxide-free organic electronic photovoltaic devices," *Org. Electron.*, vol. 15, no. 10, pp. 2624–2631, 2014.

[33] O. A. Abdulrazzaq, V. Saini, S. Bourdo, E. Dervishi, and A. S. Biris, "Organic Solar Cells: A Review of Materials, Limitations, and Possibilities for Improvement," *Part. Sci. Technol.*, vol. 31, no. 5, pp. 427–442, Sep. 2013.

[34] T. A. Skotheim, R. L. Elsenbaumer, and J. R. Reynolds, *Handbook of conducting polymers*. M. Dekker, 1998.

[35] P. Piromreun, H. Oh, Y. Shen, G. G. Malliaras, J. C. Scott, and P. J. Brock, "Role of CsF on electron injection into a conjugated polymer," *http://oasc12039.247realmedia.com/RealMedia/ads/click_lx.ads/www.aip.org/pt/adcenter/pdfcover_test/L-37/1711906919/x01/AIP-PT/APL_ArticleDL_092017/scilight717-1640x440.gif/434f71374e315a556e61414141774c75?x*, Oct. 2000.

[36] T. Bülow, H. Gargouri, M. Siebert, R. Rudolph, H.-H. Johannes, and W. Kowalsky, "Moisture barrier properties of thin organic-inorganic multilayers prepared by plasma-enhanced ALD and CVD in one reactor," *Nanoscale Res. Lett.*, vol. 9, no. 1, p. 223, 2014.

[37] "Toward high performance inverted polymer solar cells," *Polymer (Guildf).*, vol. 53, no. 24, pp. 5437–5448, Nov. 2012.

[38] D. E. Markov, E. Amsterdam, P. W. M. Blom, A. B. Sieval, and J. C. Hummelen, "Accurate Measurement of the Exciton Diffusion Length in a Conjugated Polymer Using a Heterostructure with a Side-Chain Cross-Linked Fullerene Layer."

[39] Y. Tamai, H. Ohkita, H. Benten, and S. Ito, "Exciton Diffusion in Conjugated Polymers: From Fundamental Understanding to Improvement in Photovoltaic Conversion Efficiency," *J. Phys. Chem. Lett.*, vol. 6, no. 17, pp. 3417–3428, Sep. 2015.

[40] "National Instruments: Test, Measurement, and Embedded Systems - National Instruments." [Online]. Available: http://www.ni.com/en-us.html. [Accessed: 19-Oct-2017].

[41] "Lights-Out Solar Power." [Online]. Available: http://www4.evaluationengineering.com/lights-out-solar-power. [Accessed: 19-Oct-2017].

[42] "Solar Cell I-V Characteristic and Solar I-V Curves." [Online]. Available: http://www.alternative-energy-tutorials.com/energy-articles/solar-cell-i-v-characteristic.html. [Accessed: 10-Oct-2017].

[43] "PVEducation." [Online]. Available: http://pveducation.org/. [Accessed: 19-Oct-2017].

[44] G. Ghibaudo, Q. Rafhay, G. Ghibaudo, and Q. Rafhay, "Electron and Hole Mobility in Semiconductor Devices," in *Wiley Encyclopedia of Electrical and Electronics Engineering*, Hoboken, NJ, USA: John Wiley & Sons, Inc., 2014, pp. 1–13.

[45] Y. H. Kim, C. Sachse, M. L. Machala, C. May, L. Müller-Meskamp, and K. Leo, "Highly Conductive PEDOT:PSS Electrode with Optimized Solvent and Thermal Post-Treatment for ITO-Free Organic Solar Cells," *Adv. Funct. Mater.*, vol. 21, no. 6, pp. 1076–1081, Mar. 2011.

[46] Z. Zhu, C. Liu, J. Xu, Q. Jiang, H. Shi, and E. Liu, "Improving the electrical conductivity of PEDOT:PSS films by binary secondary doping," *Electron. Mater. Lett.*, vol. 12, no. 1, pp. 54–58, Jan. 2016.